Diffusion in multi-dimensional solids using Forman's combinatorial differential forms

Applied Mathematical Modelling 110 (2022) 172–192

Contents lists available at ScienceDirect

Applied Mathematical Modelling

journal homepage: www.elsevier.com/locate/apm

Diffusion in multi-dimensional solids using Forman's combinatorial differential forms

Kiprian Berbatov[a,*], Pieter D. Boom[a], Andrew L. Hazel[b], Andrey P. Jivkov[a]

[a] Department of Mechanical, Aerospace and Civil Engineering, The University of Manchester, Oxford Road, Manchester M13 9PL, UK
[b] Department of Mathematics, The University of Manchester, Oxford Road, Manchester M13 9PL, UK

ARTICLE INFO

Article history:
Received 16 January 2022
Revised 24 May 2022
Accepted 27 May 2022
Available online 2 June 2022

Keywords:
Discrete topology
Metric operations
Transport in complex solids
Carbon nano-tubes
Graphene nano-plates

ABSTRACT

The formulation of combinatorial differential forms, proposed by Forman for analysis of topological properties of discrete complexes, is extended by defining metric-dependent operators: discrete metrics, inner products, Hodge star operators, and codifferentials on forms. These are used to build an intrinsic description of physical processes dependent on scalar variables, and the corresponding boundary value problems. The description does not assume the existence of smooth vector fields and forms extrinsic to the discrete complex. The result is a discrete formulation of physical balance laws, not another method for discretising continuum problems. Importantly, the proposed formulation provides a significant new modelling capability: physical processes may be set to operate differently on cells with different dimensions within a complex. An application of the new method to the heat/diffusion equation is presented to demonstrate how it captures the effect of changing properties of microstructural elements on the macroscopic behavior. The proposed method is applicable to a range of physical problems, including heat, mass and charge diffusion, and flow through porous media.

1. Introduction

Approximating solid materials as continua simplifies the mathematical descriptions of the physical and mechanical processes operating on them, and of the corresponding conservation laws. These descriptions are typically partial differential equations and their solutions, mostly numerical and rarely analytical, have been serving well all branches of engineering for over two centuries. However, real solids have internal structures, where the "continuum" bulk is broken down into discrete regions by "defects". These "defects" may be introduced by design, for example particles, fibres or platelets of materials different from the bulk are dispersed or arranged to form composites [1], or by the manufacturing process, for example boundaries between crystals, junctions between boundaries, and particulate precipitates form during solidification of polycrystalline metallic alloys [2]. In a number of practical problems the properties of the bulk and the different "defect" types that control given physical or mechanical process are different. For example, the thermal conductivity, mass diffusivity, or electrical conductivity of the bulk may differ from those of the different defects to such an extent that the corresponding

* Corresponding author.
E-mail addresses: kiprian.berbatov@postgrad.manchester.ac.uk (K. Berbatov), kberbatov@gmail.com (A.P. Jivkov).

https://doi.org/10.1016/j.apm.2022.05.043

heat conduction, mass diffusion or charge transfer are either strongly localised or strongly inhibited by the defects. The rapid development of the additive manufacturing techniques for both monolithic [3] and composite [4] materials, coupled with increasing demands for multi-functional materials, calls for efficient methods for analysis of materials with such complex internal structures.

One approach to keep the continuum approximation but account for the effects of internal structures on the macroscopic/bulk behaviour is to modify the governing equations by using derivatives of fractional orders. This is the subject of fractional calculus [5], a mathematical area with a number of applications to science and engineering problems [6]. Selected examples include formulations of thermo-elasticity [7], viscoelasticity [8], mass diffusion [9], reaction-advection-diffusion [10] and autocatalytic reaction-diffussion [11] in structured media. In all cases, the fractional order of the derivatives is selected such that the results fit experimental data. Hence, fractional calculus can be seen as a way to capture the effects of the underlying structure on the process under investigation. Inversely, an order of the derivative, required to describe experimental observations but different from a natural number, indicates the existence of an underlying structure. Despite the demonstrated successes of fractional calculus, the approach lacks explanatory power, i.e., it cannot provide explanations for the relations between underlying structures and observed behaviours. Due to this limitation, fractional calculus cannot be used for rational design of internal structures. An approach that has the potential to provide such explanations needs to account explicitly for the finite and discrete nature of the defects shaping the internal structures.

At a certain length scale of observation the defects can be considered as forming 0-dimensional (particles), 1-dimensional (fibres or junctions), and 2-dimensional (platelets and boundaries) sub-structures, which may not be necessarily connected, but partially tessellate the 3-dimensional bulk. A solid with such defects can be modelled by mapping the defects to a polyhedral complex, which in the terminology of algebraic topology is a 3-complex constructed from 0-cells representing vertices, 1-cells representing line segments, 2-cells representing polygonal areas, and 3-cells representing polyhedral volumes. The mapping sends 0-dimensional defects to some 0-cells, 1-dimensional defects to some 1-cells, 2-dimensional defects to some 2-cells, and the bulk material is mapped to all 3-cells and to the unoccupied cells of lower dimensions. The question requiring investigation is how to formulate the processes and fulfill the conservation laws on such cell complexes, considering the possibility to have different physical properties for different cells.

One approach to the analysis on cell complexes (specifically simplicial complexes), known as Discrete Exterior Calculus (DEC) [12], has been developed to translate the operations of smooth exterior calculus on such complexes. The basic structures on cell complexes are the chains (a p-chain is a linear combinations of p-cells) and the cochains (a p-cochain is a linear functional on p-chains). DEC assumes smooth exterior forms living in a background (Euclidean) space and defines maps between these and the cochains on the cell complex: smooth p-forms are mapped to p-cochains. Thus, DEC is intended to be a geometric discretisation method, i.e., to discretise the continuum operators using cochains considered as discrete differential forms. From this perspective it is similar to the Finite Element Exterior Calculus [13]. DEC has been used for example to formulate transport through porous media [14] and the mathematically similar incompressible fluid flow [15]. It has been recently shown that DEC solutions of Poisson problems with existing analytical solutions, i.e., homogeneous domains with specific geometries and boundary conditions, converge to the analytical solutions with mesh refinement (increasing the number of 3-cells in the domain) [16]. This illustrates its conceptual similarity to the finite element method. A DEC-based formulation for elasticity has also been recently proposed [17].

A framework, similar to DEC, which uses primal and dual meshes, is the Compatible Discrete Operators (CDO) approach [18]. It discretises differential operators with coboundary operators and constitutive laws with discrete Hodge star operators that relate primal p-chains and dual $(d-p)$-cochains. Another framework, in the spirit of finite elements, that can be applied to polytopal meshes is the virtual element method [19]. Its difference with polynomial finite element methods is that local element spaces are defined as solutions to particular partial differential equations on polytopal domains and the shape functions are not known explicitly (the element matrices are computed approximately via projection operators). Recently, polynomial elements (of any order) on polytopal meshes have been proposed [20].

However, these approaches are not applicable to the problem at hand - analysis of processes operating differently on cells of different dimensions. Moreover, DEC's spirit is very different from what is needed for an intrinsic formulation of physics and mechanics on discrete topological spaces. Closer in spirit is the so called "cell method" advocated by Tonti [21], which seeks an *ab initio* formulation that does not rely on the existence of a smooth background space. An opportunity to develop an intrinsic formulation is presented by the works of Forman [22,23], which introduce the notions of combinatorial vector fields and differential forms. Forman's combinatorial vector fields and the associated discrete Morse theory have been used for example for computing the homology of [24] and flows on [25] cell complexes. The combinatorial differential forms have been used for constructing combinatorial Laplacians and computing combinatorial Ricci curvatures of cell complexes [26–28], which in turn have been widely used for analysis of Ricci-flows on such complexes [29].

The aim of this article is to extend Forman's approach to allow for formulating a discrete version of the heat/diffusion equation. This extension follows some ideas from the thesis of Arnold on the topological operations on cell complexes [30] and from the work of Wilson on cochain algebra [31]. The main mathematical contributions are the proposed metric operator on cochains that takes two p-cochains and returns a 0-cochain, and from there the formulations of inner product of cochains and adjoint operators to exterior differentials required to represent balance equations. Notably, the development allows formulation of physical balance laws and corresponding boundary value problems in assemblies of finite, discrete entities. This is a fundamentally different modelling approach from that of continuum theories. The main contribution to materials modelling is that the proposed method can describe materials with complex internal structures that cannot be

exactly represented by continuum theories, e.g., those where elements of different dimensions have different physical properties and the interactions between them can be finely controlled. The development is new and can be considered as a step towards an intrinsic description of structured solids. The theory will be completed once a formulation of solid deformations is presented, which is a subject of an ongoing work.

1.1. Continuum problem

The continuum version of the heat/diffusion equation, for which a discrete analogue rather than a discrete approximation is being sought, is presented to help comparisons between the continuum and discrete cases. Consider a bounded open domain $M \subset \mathbb{R}^d$, with closure $\overline{M}$ and boundary $\partial M := \overline{M} \setminus M$. With the classical vector calculus notations, the heat equation in M expressing the conservation of a scalar quantity in the absence of body sources, is given by

$$\frac{\partial u}{\partial t} + \nabla \cdot \mathbf{f} = 0, \tag{1}$$

where u is a scalar field, e.g., temperature, concentration, or charge, and $\mathbf{f}$ is a vector field, e.g., heat, mass, or charge flux. The relation between the scalar and the vector quantities at a point in M is provided by a constitutive relation of the form

$$\mathbf{f} = -\alpha \nabla u, \tag{2}$$

where α is a material property – thermal, mass, or electrical diffusivity. In the general case of anisotropic materials, α is a tensor field in M. For inhomogeneous, but isotropic materials α is a positive scalar field in M, and for homogeneous and isotropic materials $\alpha = \text{const} > 0$ across M. Irrespective of the material constitution and the dimension of the domain, d, the physical dimension of the diffusivity coefficient(s) is $[\alpha] = L^2/T$, where L and T are measures of length and time, respectively. If $[u]$ denotes the physical dimension of the scalar quantity, then the constitutive relation given by Eq. (2) gives the physical dimension of the flux as $[f] = [u]L/T$.

An initial boundary value problem is formulated by prescribing initial values of u in M and boundary conditions on ∂M. The boundary is represented as a union of non-overlapping sub-domains, ∂M_D and ∂M_N, i.e., $\partial M_D \cup \partial M_N = \partial M$ and $\partial M_D \cap \partial M_N = \varnothing$. The initial boundary value problem, including initial, Dirichlet and Neumann boundary conditions is

$$\begin{aligned}
\frac{\partial u}{\partial t} &= \nabla \cdot (\alpha \nabla u) \\
u &= u_0 \qquad t = 0 \qquad \text{in} \quad M, \\
u &= \bar{u}(t) \qquad t \geq 0 \qquad \text{on} \quad \partial M_D, \\
\mathbf{f} \cdot \mathbf{n} &= \bar{f}(t) \qquad t \geq 0 \qquad \text{on} \quad \partial M_N,
\end{aligned}$$

where $\bar{u}(t)$ is prescribed scalar quantity at a given point on ∂M_D, $\mathbf{n}$ is the outward unit normal to a given point on ∂M_N, and $\bar{f}(t)$ is prescribed flux normal to a given point on ∂M_N.

In the language of exterior differential forms, the scalar quantity u is a 0-form, and the flux $\mathbf{f}$ is a 1-form. This perspective is the bridge to the intrinsic discrete version developed in the paper with an appropriate definition of discrete differential forms together with topological and metric operations on such forms substituting the continuum gradient and divergence. The formulation requires background knowledge of discrete complexes or meshes, as well as of topological and metric operations on meshes. So far the required mathematical apparatus is not as widely known and used as the continuum calculus, and every effort is made to explain its components by formulas and examples.

1.2. Overview of the paper

The purpose of this section is to provide a summary of the notions discussed in this paper. The key steps of the development are presented in the main text and should be accessible to readers familiar with the standard notions of polytopes, meshes, orientation, and the boundary operator on meshes. For readers less familiar with these notions, polytopes and meshes are introduced in Appendix A, and orientations and boundary operators are introduced in Appendix B, given as supplementary material. They are also available in the preprint version of the paper at https://arxiv.org/abs/2201.03704. Section 2 summarises and generalises notions considered in [23] and [30], such as discrete differential forms, Forman subdivision and cubical cup product. Important for this work is the idea of using the Forman subdivision to model physical problems. Section 3 is the main theoretical contribution, in particular the use of a metric tensor (and node curvature) to define an inner product and related notions. Appendix C summarises standard topological results that use, but are independent of, an inner product. It can be read independently of Section 3 and the results there do not affect the rest of the paper, but are included for the benefit of interested readers. The application of the developed intrinsic theory is provided in Section 4 by several numerical examples, demonstrating its use for analysis of materials with complex internal structures. More detailed explanations of the notions in various sections of the paper are presented in the following paragraphs.

Key notions from Appendix A A flat region is a d-manifold embeddable in a d-dimensional affine space. A d-polytope is recursively defined as a flat region, homeomorphic to an open set in $\mathbb{R}^d$, whose boundary is a union of finite number of $(d-1)$-polytopes, with 0-polytopes being points. According to this definition, regions with holes and self-intersecting regions are excluded, but non-convex regions are allowed. A d-polytope will be referred to as d-cell, with 0,1,2,3-cells occasionally called

nodes (N), edges (E), faces (F), and volumes (V), respectively. A hyperface of a d-cell c_d is one of the $(d-1)$-cells, forming the boundary of c_d. A p-face of c_d, $0 \leq p \leq d$ is a p-cell b_p such that there exists a sequence of cells starting from b_p and finishing at c_d with every element in the chain being a hyperface of the next one. In this case we say that c_d is a superface of b_p.

A d-mesh is a collection of cells with maximal topological dimension d such that any two cells can intersect in a finite (possibly empty) union of other cells. The topological dimension of a mesh is the maximal dimension of its cells. The embedding dimension of a mesh is the dimension of the affine space the mesh is embedded in. The embedding dimension is not important when looking intrinsically at the mesh. A manifold-like mesh is a d-mesh representing a topological manifold. A crucial property is that all $(d-1)$-cells have at most two d-superfaces.

Key notions from Appendix B An orientation of a cell is a choice of equivalence class of homotopical bases, i.e., all the bases that can be continuously deformed from one another. There are two such classes. A different definition using top-dimensional elements of the exterior algebra is presented in order to include the 0-cells. Furthermore, it allows easier algebraic manipulations.

The relative orientation between two cells c_p and b_{p-1} is a choice of 1 or -1 depending on the chosen orientations of c_p and b_{p-1} and any outward-pointing vector to b_{p-1} with respect to c_p. A compatible orientation on a manifold-like mesh M is an orientation on M such that for any pair of d-cells with a common hyperface b_{d-1}, their relative orientations with respect to b_{d-1} are opposite. If a compatible orientation on M exits, M is called compatibly orientable. If a compatible orientation on M is chosen, M is called compatibly oriented.

A chain is a formal linear combination of the cells of the complex. In general, the coefficients of the linear combination can belong to a ring, but in this work they are considered to be elements of $\mathbb{R}$. The boundary operator ∂ is a linear map between chains which, applied to a basis cell, returns a linear combination of its boundary faces with coefficients 1 and -1 given by the relative orientations. The boundary operator satisfies $\partial \circ \partial = 0$, where $\circ$ denotes composition of functions, which makes the collection of chain spaces a chain complex. The fundamental class $[M]$ on a compatibly oriented manifold-like mesh M is the sum of all of its d-cells. A cochain is a linear functional on chains. The coboundary operator δ is the dual to the boundary map and induces a cochain complex.

Key notions from Section 2 A discrete differential p-form is a linear map between chains which, when applied to a basis chain (cell) b_q, gives a linear combination of the basis $(q-p)$-chains which are faces of b_q. The discrete exterior derivative, D, is a linear map taking p-forms to $(p+1)$-forms and satisfying $D \circ D = 0$.

A d-polytope is a simple polytope if any of its nodes is connected to exactly d edges. The Forman subdivision of a mesh M is a mesh K (a subdivision of M) such that the cochains in K correspond to the discrete differential forms in M. A (compatible) orientation on M induces a (compatible) orientation on K.

Two polytopes are called combinatorially equivalent if there is a bijection between their cells that respects the boundary. A (d-dimensional) quasi-cube is a polytope which is combinatorially equivalent to a (d-dimensional) cube. The quasi-cubical cup product is a bilinear map in the cochain complex of a quasi-cubical mesh which satisfies the graded Leibniz rule with respect to D. The wedge product on a mesh M of simple polytopes is a bilinear product of forms defined by the "pullback" of the cup product on the Forman subdivision K of M.

The definition of discrete differential forms makes it clear that in the physical problem at hand, the quantity u (a 0-form) assigns a real number to b_p for $0 \leq p \leq d$, and the quantity $\mathbf{q}$ (a 1-form) assigns a real number to (c_p, b_{p-1}) for $0 < p \leq d$, where b_{p-1} is a hyperface of c_p.

Key notions from Section 3 Let M be a mesh of convex simple polytopes and K be the Forman subdivision. For a fixed inner product $\langle \cdot, \cdot \rangle$ on $C^\bullet K$ the following linear maps are constructed: adjoint coboundary operator $\delta^\star$; Laplacian Δ; Hodge star $\star$. These can be bijectively transformed to maps on $\Omega^\bullet M$.

A discrete metric tensor g is a bilinear map on K taking a pair of p-cohains and returning a 0-cochain. A family of metric tensors is constructed via a dimensionless function on the nodes accounting for a possible curvature κ of the nodes. The volume cochain vol (on K - compatibly oriented) is the d-cochain with coefficients the measures of d-cells. The Riemann integral of a zero-cochain σ^0 is the real number $(\sigma^0 \smile \mathrm{vol})[K]$. An inner product, used in this article, is given by the Riemann integral of the metric tensor.

Key notions from Appendix C For any metric on a mesh K there is a bijection between the cohomology and the kernel of Δ (the set of harmonic cochains). For a closed mesh (mesh without a boundary) with cup product and Hodge star, Poincaré duality gives bijection between homology and cohomology.

1.3. Notation and conventions

Let A be an affine space and $X \subset A$, $x_1, \ldots, x_n \in A$.

- $\mathrm{Aff}(X)$ denotes the affine hull of X; $\mathrm{Aff}(x_1, \ldots, x_n) := \mathrm{Aff}(\{x_1, \ldots, x_n\})$.
- $\mathrm{Con}(X)$ denotes the convex hull of X; $\mathrm{Con}(x_1, \ldots, x_n) := \mathrm{Con}(\{x_1, \ldots, x_n\})$.

Let M be a mesh with topological dimension $d > 0$. Variables $p, q \in \{0, \ldots, d\}$ are used to denote cell dimensions. Other standard variable names used throughout the paper include:

- $a_p, b_p, c_p \in M_p$ denote p-cells in M. By abuse of notation they denote basis p-chains;

- $\pi_p, \rho_p, \sigma_p \in C_pM$ denote p-chains in M;
- a^p, b^p, c^p denote basis p-cochains in M;
- $\pi^p, \rho^p, \sigma^p \in C^pM$ denote p-cochains in M;
- $\omega^p, \eta^p \in \Omega^pM$ denote discrete differential p-forms in M.

For $p \preceq q$ we write $a_p \preceq b_q$ (equivalently $a^p \preceq b^q$, $b_q \succeq a_p$, $b^q \succeq a^p$) if $a_p = b_q$ (hence $p = q$) or a_p is a face of b_q (hence $p \prec q$). In the later case we write $a_p \prec b_q$ (and similarly in the other 3 cases).

2. Topological operations on a mesh

This section introduces some topological operations (of algebraic nature) on a mesh M, i.e., operations which do not depend on the coordinates/embedding of the mesh but only on the connections between cells and on the orientation. They give a richer mesh calculus which allows for defining metric properties in Section 3. In [23] Forman introduced discrete (combinatorial) vector fields and differential forms and exterior derivative of forms. In the beginning of the proof of [23, Theorem 1.2] he briefly, but not sufficiently rigorously, described a mesh subdivision of M. We refer to this as the Forman subdivision of M and denote it by K. Notably, Forman did not use this subdivision anywhere else. Arnold in [30] noted that for M simplicial, K consists of topological cubes (she called the cells of K kites [30, Definition 2.1.11] and K itself the associated kite complex [30, Definition 5.2.8]) for which she developed a cup product and a topological theory, taking also inspiration from Wilson's work on simplicial meshes [31]. See Remark 2.16 for a further review of the cited literature.

2.1. Discrete differential forms

Let $C_\bullet M = \bigoplus_{p=0}^{d} C_pM$ be the space of all chains.

Definition 2.1. A discrete differential p-form is a map $\omega : C_\bullet M \to C_\bullet M$ with the properties

1. ω is a $\mathbb{R}$-linear map;
2. for each $q \geq p$, $\omega[C_q(M)] \subseteq C_{q-p}(M)$, i.e., ω is a map of degree $(-p)$ on $C_\bullet M$;
3. for each $q > p$ and $c_q \in M_q$, $\omega(c_q) \in \operatorname{span}(\{b_{q-p} \in M_{q-p} \mid b_{q-p} \preceq c_q\})$, i.e., the map is local.

The space of all p-forms on M is denoted by Ω^pM and the space of discrete differential forms $\Omega^\bullet M$ is the graded vector space $\Omega^\bullet M = \bigoplus_{p=0}^{d} \Omega^pM$.

For short, "forms" is used instead of "discrete differential forms".

Remark 2.2. Let $f : M \to \mathbb{R}$, i.e., f takes all cells as arguments. Then f gives rise to a 0-form $\mathfrak{f} : C_\bullet M \to C_\bullet M$ defined on a basis p-chain c_p as $\mathfrak{f}(c_p) = f(c_p)c_p$. Inversely, a 0-form $\mathfrak{f}$ corresponds to a function $f : M \to \mathbb{R}$, by taking the coefficient before $\mathfrak{f}(c_p)$ as the value of $f(c_p)$. Indeed, the definition of forms guarantees that the a 0-form applied to a p-cell c_p gives a linear combination of the p-faces of c_p, i.e., c_p multiplied by a number.

Example 2.3. Canonical examples of discrete differential forms include:

1. the identity function $\imath_M$ on $C_\bullet M \to C_\bullet M$ is a 0-form which corresponds to the constant function $\imath_M : M \to \mathbb{R}$, $\imath_M(c_p) = 1$;
2. the boundary map ∂ is a 1-form. Indeed: it is linear; it maps p-chains to $(p-1)$-chains; when applied to a p-cell c_p it gives a linear combination (with coefficients ± 1) of the boundary $(p-1)$-faces of c_p.

Remark 2.4. The standard basis of Ω^pM consists of the forms of the type $(c_q \to b_{q-p})$, where $b_{q-p} \preceq c_q$, defined for any $a_r \in M_r$ by

$$(c_q \to b_{q-p})(a_r) := \begin{cases} 0, & a_r \neq c_q \\ b_{q-p}, & a_r = c_q \end{cases}. \tag{3}$$

The form is extended by linearity for any $\sigma \in C_\bullet M$. In other words, a basis p-form is nonzero at exactly one of the cells c_q of M and applied to this cell gives one of its $(q-p)$-faces b_{q-p}.

Definition 2.5. Let (M, or) be an oriented mesh, $(C_\bullet M, \partial)$ be the associated chain complex. The discrete exterior derivative is the linear map $D : \Omega^\bullet M \to \Omega^\bullet M$, defined on p-forms by

$$D^p\omega^p = \omega^p \circ \partial - (-1)^p \partial \circ \omega^p \in \Omega^{p+1}M. \tag{4}$$

Remark 2.6. In [23] the map is defined by

$$D^p\omega^p = \partial \circ \omega^p - (-1)^p \omega^p \circ \partial,$$

i.e., the definition here differs by sign of $(-1)^p$. The choice adopted here does not affect the essential properties of D but has the benefit that the orientation of the Forman mesh of M, defined by using Eq. (5), inherits the orientation of M in a natural geometric way.

Example 2.7. For the canonical 1-form, ∂, it is trivial to see that $D\partial = 0$. Indeed, $D\partial = \partial \circ \partial - (-1)^1 \partial \circ \partial = 0 + 0 = 0$.

Proposition 2.8. *$D^2 = 0$, i.e., $(\Omega^\bullet M, D)$ is a cochain complex.*

Proof. It is enough to prove the proposition for p-forms for any p. Let $\omega = \omega^p \in \Omega^p M$. Then

$$\begin{aligned} D(D\omega) &= D(\omega \circ \partial - (-1)^p \partial \circ \omega) \\ &= ((\omega \circ \partial) \circ \partial - (-1)^{p+1} \partial \circ (\omega \circ \partial)) - (-1)^p ((\partial \circ \omega) \circ \partial - (-1)^{p+1} \partial \circ (\partial \circ \omega)) \\ &= 0 + (-1)^p \partial \circ \omega \circ \partial - (-1)^p \partial \circ \omega \circ \partial + 0 \\ &= 0. \end{aligned}$$

□

2.2. Forms as cochains on the Forman subdivision

The expression for $D^p \omega^p$ for a basis p-form $\omega^p = (c_q \to b_{q-p})$ is given by

$$\begin{aligned} D^p \omega^p &= D^p (c_q \to b_{q-p}) \\ &= (c_q \to b_{q-p}) \circ \partial - (-1)^p \partial \circ (c_q \to b_{q-p}) \\ &= \sum_{a \in M} (c_q \to b_{q-p})(\partial a) - \sum_{a \in M} (-1)^p \partial ((c_q \to b_{q-p})(a)) \\ &= \sum_{a_{q+1} \succ c_q} \varepsilon(a_{q+1}, c_q)\ (a_{q+1} \to b_{q-p}) - (-1)^p \sum_{a_{q-p-1} \preceq b_{q-p}} \varepsilon(b_{q-p}, a_{q-p-1})\ (c_q \to a_{q-p-1}). \end{aligned} \tag{5}$$

For mesh M with convex cells, Eq. (5) has a nice interpretation on a subdivision K of M, which is referred to as the Forman subdivision of M. K is constructed as follows:

- to any q-cell c_q of M ($0 \le q \le d$) corresponds a vertex (a geometric point) in K – usually in the interior of c_q;
- to any pair (c_q, b_{q-p}) in M with $b_{q-p} \preceq c_q$ corresponds a p-cell in K (when $p = 0$, $b_q = c_q$ and hence to c_q in M corresponds a 0-cell in K, agreeing with the above construction of vertices);
- a p-cell (c_q, b_{q-p}) in K is a hyperface of the cells of the type (a_{q+1}, b_{q-p}) for $a_{q+1} \succ c_q$ and (c_q, a_{q-p-1}) for $a_{q-p-1} \preceq b_{q-p}$ (thus, ensuring we have the full topology: the edges that the nodes are connected to, the faces that the edges are connected to, etc.).

Thus, the topology of K is uniquely constructed and only positions of nodes have to be specified to fully recover the mesh. K also inherits orientation from M as follows:

- the nodes are given positive orientations but the orientations of the p-cells for $p \ge 1$ are not given directly – they are inferred from the relative orientations using the coefficients in Eq. (5) as follows. With the notation from the previous point the relative orientation between (a_{q+1}, b_{q-p}) and (c_q, b_{q-p}) is $\varepsilon(a_{q+1}, c_q)$, while the relative orientation between (c_q, a_{q-p-1}) and (c_q, b_{q-p}) is $(-1)^{p+1}\varepsilon(b_{q-p}, a_{q-p-1})$. With this information we construct the absolute orientations of edges (from nodes), faces (from edges), volumes (from faces), etc. recursively; (Indeed, consider a p-polytope c_p, an oriented hyperface b_{p-1} of it, and a number $s \in \{-1, 1\}$. Then there exists a unique orientation of c_p such that $\varepsilon(c_p, b_{p-1}) = s$.)
- the forms on M correspond to the cochains of K and the coboundary operator on K is given by the same formula as in Eq. (5). δ_K is a valid coboundary operator, since $\delta_K \circ \delta_K = 0$, and δ_K has the topological structure of a coboundary operator (1 or -1 for adjacent cells and 0 otherwise).

For the topological operations on a mesh, the geometric positions of the 0-cells of K with respect to the corresponding p-cells of M is irrelevant. However, for the metric operations these positions are essential. The choice adopted here is to place the 0-cells of K at the centroids of the corresponding p-cells of M. It is not claimed that this choice is optimal, but it is used in the numerical simulations presented later.

Definition 2.9. Call the constructed bijection between $\Omega^\bullet M$ and $C^\bullet K$ the Forman isomorphism F. Indeed, it provides an isomorphism

$$(\Omega^\bullet M, D) \cong (C^\bullet K, \delta).$$

Example 2.10. Figure 1 shows: (a) M - a square divided into two triangles region; and (b) K - the Forman subdivision of M. Both meshes are numerated and oriented; the orientation of K is the induced one as discussed. Different colours are used for different types of p-cells in K:

The nodes in K: from 1 to 4 coincide with those in M; from 5 to 9 are the midpoints of the edges of M; and 10 and 11 are the centroids of the faces of M. The nodes in K are coloured according to the colour of the original cell they represent.

The edges in K: from 1 to 10 correspond to edge-node pairs in M; from 11 to 16 correspond to face-edge pairs. Different colours are used for the two different types of edges.

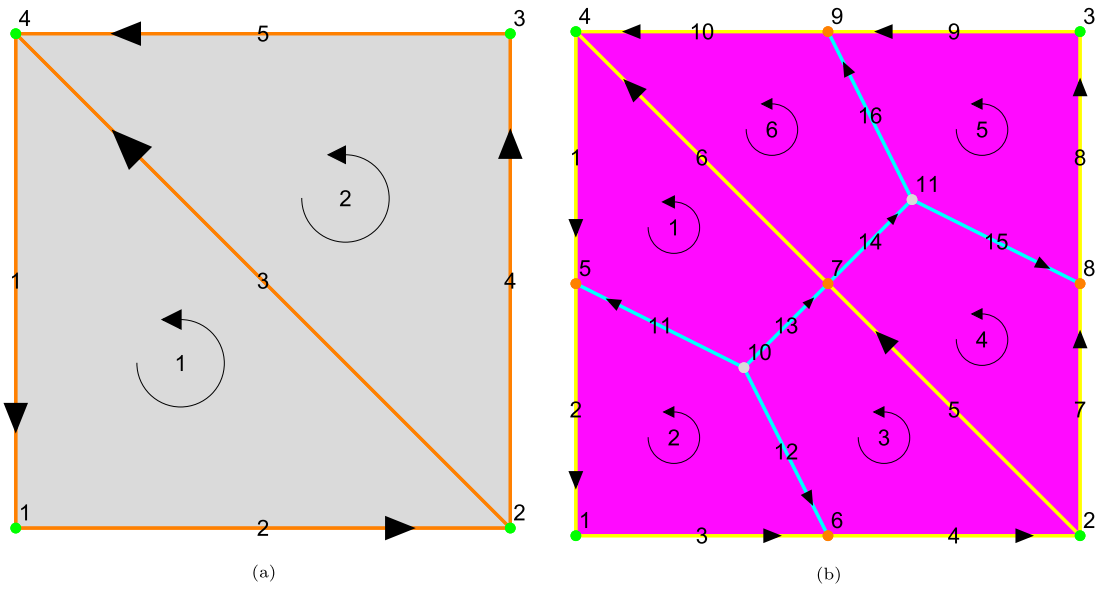

Fig. 1. Triangulation (a) and its Forman subdivision (b).

The faces in K correspond to face-node pairs in M.

Regarding orientation, the following examples using Eq. (5) are given (they are consistent with the drawn orientation of the cells of K). Note that the nodes (N), edges (E) and faces (F) correspond to those in M:

$$\begin{aligned} D^0(E_3 \to E_3) &= \varepsilon(F_1, E_3)(F_1 \to E_3) + \varepsilon(F_2, E_3)(F_2 \to E_3) - \varepsilon(E_3, N_2)(N_3 \to E_2) - \varepsilon(E_3, N_4)(E_3 \to N_4) \\ &= (F_1 \to E_3) - (F_2 \to E_3) + (E_2 \to N_3) - (E_3 \to N_4) \end{aligned}$$

which in K corresponds to $\delta^0_K N^7 = E^{13} - E^{14} + E^5 - E^6$;

$$D^0(F_1 \to E_1) = \varepsilon(E_1, N_1)(F_1 \to N_1) + \varepsilon(E_1, N_4)(F_1 \to N_4) = (F_1 \to N_1) - (F_1 \to N_4)$$

which in K corresponds to $\delta^1_K E^{11} = F^2 - F^1$;

$$D^0(E_4 \to N_3) = \varepsilon(F_2, E_4)(F_2 \to N_3) = (F_2 \to N_3)$$

which in K corresponds to $\delta^1_K E^8 = F^5$.

Remark 2.11. The geometric construction of K is not suitable for all types of convex meshes with $d > 2$. For example for any convex mesh M with $d = 2$ the resulting K consists of quadrilaterals, but for a convex mesh M with $d > 2$ several outcomes for K are possible. It is sufficient to consider M as a single 3-cell. The possible outcomes for K are illustrated in Fig. 2:

- if M is a parallelepiped, then K consists of 8 equal parallelepipeds (Fig. 2a);
- if M is a tetrahedron, then any K consists of 4 hexahedrons, referred to as quasi-cubes (Fig. 2b);
- if M is a general simple polyhedron (a simple 3-polytope), then K consists only of quasi-cubes. However, the faces with one vertex at the centroid of M may be non-planar quadrilaterals. Hence, K may not be strictly a polytopal mesh (Fig. 2c);
- if M is not a simple polyhedron, then K is not quasi-cubical and the theory developed in this work does not apply (Fig. 2d).

The developments in this work exclude meshes having at least one cell which is not a simple polytope, so that K is always a quasi-cubical mesh (otherwise the definition of cup product given in Definition 2.12 becomes useless - for instance, it does not satisfy the graded Leibniz rule in Theorem 2.14). Furthermore, if K is not strictly polytopal, the areas of non-planar quadrilaterals are found by dividing these quadrilaterals into two triangles and summing up the two areas.

2.3. Quasi-cubical cup product of cochains and wedge product of forms

The following is a generalisation of [30, Definition 3.2.1] from cubes to arbitrary quasi-cubes.

Definition 2.12. Let K be an oriented quasi-cubical mesh. The quasi-cubical cup product is the unique bilinear map $\smile$: $C^\bullet K \times C^\bullet K \to C^\bullet K$ (with $\pi^p \smile \rho^q \in C^{p+q}K$) defined for basis cochains a^p and b^q as follows.

- If $a_p \cap b_q = \emptyset$ or $\dim(\mathrm{Aff}(a_p \cup b_q)) < p + q$, then $a^p \smile b^q := 0$.

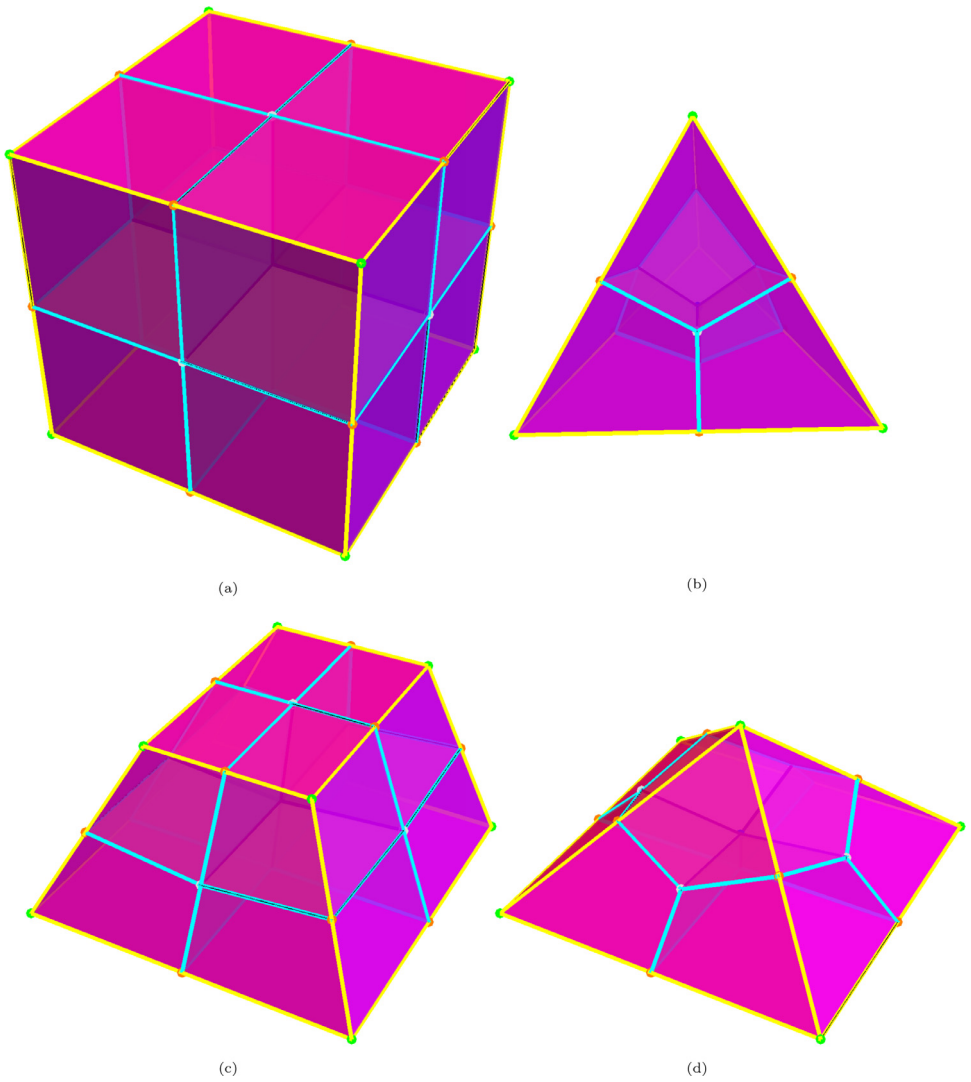

Fig. 2. The Forman subdivision of: (a) cube; (b) tetrahedron; (c) hexahedron; (d) square pyramid.

- If $a_p \cap b_q \neq \emptyset$ and $\dim(\mathrm{Aff}(a_p \cup b_q)) = p+q$, in which case $a_p \cap b_q$ is a point, then since K is a convex mesh there exists at most one $c_{p+q} \in K_{p+q}$ such that $c_{p+q} \succeq a_p$ and $c_{p+q} \succeq b_q$. If there is no such c_{p+q}, then again $a^p \smile b^q := 0$. If there is such c_{p+q}, then

$$a^p \smile b^q := \frac{1}{2^{p+q}} \frac{\mathrm{or}(a_p) \wedge \mathrm{or}(a_q)}{\mathrm{or}(c_{p+q})}\ c^{p+q}. \tag{6}$$

  In this formula, $\wedge$ denotes the wedge product of the exterior algebra and $\mathrm{or}(\alpha)$ is the orientation of a cell α as discussed in Appendix B.2.

Example 2.13. Some values of the cup product of basis cochains are given in Fig. 3a.
$N^6 \smile N^6 = N^6$, $N^2 \smile E^{16} = E^{16} \smile N^2 = E^{16}/2$, $N^{16} \smile F^8 = F^8 \smile N^{16} = F^8/4$.
$E^5 \smile E^{10} = -E^{10} \smile E^5 = F^{12}/4$.
$E^7 \smile E^8 = 0$ because the 1-cells do not share a common 2-cell, although they intersect.
$E^7 \smile E^{22} = 0$ because the 1-cells do not intersect, although they share a common 2-cell.

Let $\overline{1_M} := F(1_M)$. The theorem below ensures that $\smile$ is an abstract cup product in the sense of [30, Definition 2.3.2] (the statement of the theorem and its proof can be found in [30, Theorem 3.2.3]).

Theorem 2.14. *$\smile$ satisfies the following properties:*

1. *if $a^p \smile b^q$ is nonzero, then a_p and b_q are faces of a common $(p+q)$-cell;*

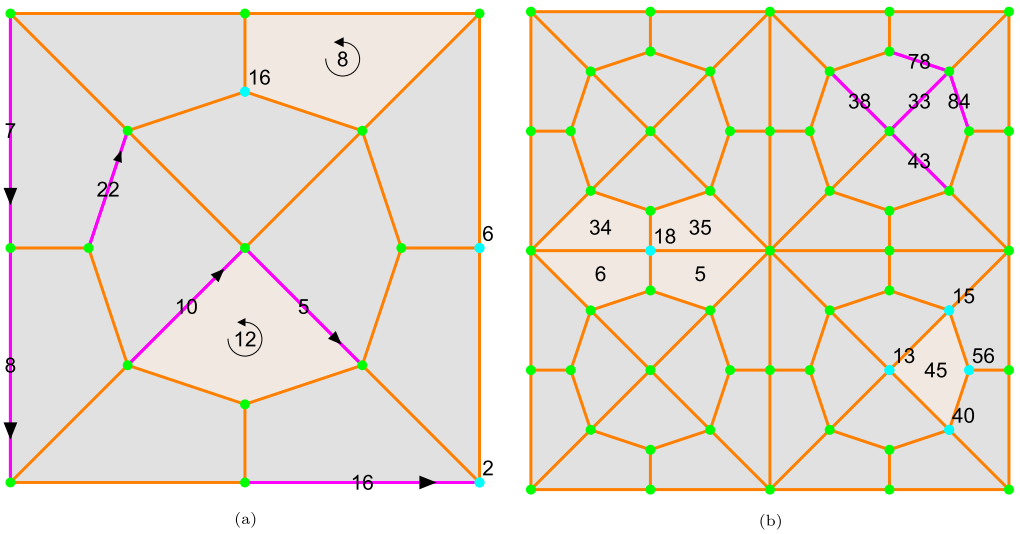

Fig. 3. Examples of: (a) cup product; (b) Hodge star.

2. $\delta(a^p \smile b^q) = (\delta a^p) \smile b^q + (-1)^p a^p \smile (\delta b^q)$ *(graded Leibniz rule);*
3. $\overline{1_M} \cup a^p = a^p \cup \overline{1_M} = a^p$.

Definition 2.15. Let M be an oriented mesh of simple polytopes and $\smile$ be the cup product on the Forman subdivision K. The discrete wedge product is the bilinear map $\wedge : \Omega^\bullet M \times \Omega^\bullet M \to \Omega^\bullet M$ (with $\omega^p \wedge \eta^q \in \Omega^{p+q} M$) defined on basis forms by "transporting" the definition of the cup product using the Forman isomorphism F:

$$\omega^p \wedge \eta^q := F^{-1}(F(\omega^p) \smile F(\eta^q)). \tag{7}$$

The following identities are transformed from $C^\bullet K$ to $\Omega^\bullet M$ using F^{-1}.

$$1_M \wedge \ \omega = \omega \wedge 1_M = \omega. \tag{8}$$

$$D(\omega^p \wedge \eta^q) = (D\omega^p) \wedge \eta^q + (-1)^p \omega^p \wedge (D\eta^q). \tag{9}$$

$$(\Omega^\bullet M, \wedge, D) \cong (C^\bullet K, \smile, \delta). \tag{10}$$

Remark 2.16. Scott Wilson introduced a similar cup product on simplicial meshes [31, Definition 5.1] using Whitney forms [32]. He then proved that they were purely combinatorial, i.e., did not depend on the coordinates of the nodes [31, Theorem 5.2]. He also showed that for suitable mesh refinements, the cochains are approximations of smooth differential forms. Rachel Arnold defined a cup on cubes [30, Definition 3.2.1] and showed [30, Theorem 3.2.12] that it coincided with the cup product defined using cubical Whitney forms [30, Definition 3.2.10]. She did not define it in the general form for quasi-cubes shown in Definition 2.12. On the other hand, she defined a product of discrete forms on M [30, Definition 5.4.1] and constructed a cup product on K [30, Definition 5.4.3] using the Forman isomorphism. This is in contrast to our approach, when we start with an arbitrary polytopal mesh M (of simple polytopes) and use the combinatorial regularity of K to define the cup product there and to "pull it back" to a wedge product on M.

3. Discrete metric operations

This section develops mesh operations requiring an additional structure on a mesh, namely an inner product. This allows to define adjoint coboundary operator, Laplacian and Hodge star, which have been explored in the literature but mainly for: (1) topological results independent of the choice of an inner product, such as the discrete Hodge theory discussed in Appendix C.1 and Appendix C.2 and the discrete Poincaré duality referenced in Appendix C.3; and (2) convergence results dependent on a particular choice of an inner product - this is discussed in [31].

The main goal here is to define an inner product and its derivative notions suitable for solving physical problems. The novelty is the introduction of a discrete metric tensor (in fact, a whole class of metrics) and the resulting inner product defined via Riemann integration along a volume cochain. The theory is then applied to physical problems in Section 4.

The section is developed from general to specific. First, the adjoint coboundary operator, $\delta^\star$, the Laplacian, Δ, and the Hodge star operator, $\star$, are defined in Section 3.1 for a general choice of an inner product, $\langle\cdot,\cdot\rangle$. These ingredients are sufficient for development of a topological theory - Appendix C. Second, explicit formulas for $\delta^\star$, Δ and $\star$ are given in Section 3.2 for the case where the basis cochains form an orthogonal basis of C^pK with respect to $\langle\cdot,\cdot\rangle$. The most important contribution is in Section 3.3 where a class of metric tensors is proposed leading to dimensional orthogonal inner products.

3.1. General inner product

Let $\langle\cdot,\cdot\rangle : C^pK \times C^pK \to \mathbb{R}$ be an inner product (symmetric and positive definite bilinear map).

Definition 3.1. The adjoint coboundary operator $\delta^\star_{p+1} : C^{p+1}K \to C^pK$ is defined as the adjoint of δ_p, i.e., for any $\sigma^p \in C^pK,\ \tau^{p+1} \in C^{p+1}K$,

$$\langle \delta_p \sigma^p, \tau^{p+1}\rangle = \langle \sigma^p, \delta^\star_{p+1}\tau^{p+1}\rangle. \tag{11}$$

Definition 3.2. The discrete Laplacian is given by

$$\Delta_p = \delta_{p-1}\circ\delta^\star_p + \delta^\star_{p+1}\circ\delta_p. \tag{12}$$

Definition 3.3. The discrete Hodge star on p-forms is the unique map $\star : C^pK \to C^{d-p}K$ such that for any $\sigma^{d-p} \in C^{d-p}K,\ \tau^p \in C^pK$,

$$\langle \sigma^{d-p}, \star_p \tau^p\rangle = (\sigma^{d-p} \smile \tau^p)[K], \tag{13}$$

where $[K]$ is the fundamental class of the compatibly oriented manifold-like mesh K.

3.2. Orthogonal inner product

When the basis cochains form an orthogonal basis with respect to the inner product, the operations introduced in Section 3.1 have nice closed forms. Similar formulas are derived in [26, Section 2] where the adjoint coboundary operator and the Laplacian are defined on the chains of M and the values of the inner product at basis chains are called weights.

Adjoint coboundary operator To compute $\delta^\star$, let

$$\delta^\star_{p+1} c^{p+1} = \sum_{b^p} \lambda_{b^p} b^p$$

for the unknown coefficients $\lambda_{b^p} \in \mathbb{R}$. Then

$$\langle \delta_p a^p, c^{p+1}\rangle = \langle a^p, \delta^\star_{p+1} c^{p+1}\rangle = \langle a^p, \sum_{b^p} \lambda_{b^p} b^p\rangle = \lambda_{a^p}\langle a^p, a^p\rangle.$$

Hence, $\lambda_{a^p} = \langle \delta_p a^p, c^{p+1}\rangle / \langle a^p, a^p\rangle$ and therefore

$$\delta^\star_{p+1} c^{p+1} = \sum_{a^p} \lambda_{a^p} a^p = \sum_{a^p} \frac{\langle \delta_p a^p, c^{p+1}\rangle}{\langle a^p, a^p\rangle} a^p = \sum_{a^p \prec c^{p+1}} \varepsilon(c_{p+1}, a_p) \frac{\langle c^{p+1}, c^{p+1}\rangle}{\langle a^p, a^p\rangle} a^p. \tag{14}$$

The matrix stencil of the adjoint coboundary operator with respect to the standard bases of C^pK and $C^{p+1}K$ is the same as the one of the boundary operator with respect to the standard bases of chains of C_pK and $C_{p+1}K$. Moreover, the signs are also the same as is evident by Eq. (14) and the positive-definiteness of the inner product.

Laplacian of 0-chains

$$\begin{aligned}
\Delta_0 c^0 = \delta^\star_1(\delta_0 c^0) &= \delta^\star_1\left(\sum_{b_1 \succ c_0} \varepsilon(b_1, c_0)\, b^1\right) \\
&= \sum_{b_1 \succ c_0}\sum_{a_0 \prec b_1} \varepsilon(b_1, c_0)\,\varepsilon(b_1, a_0)\,\frac{\langle b^1, b^1\rangle}{\langle a^0, a^0\rangle} a^0 \\
&= \frac{1}{\langle c^0, c^0\rangle}\left(\sum_{b_1 \succ c_0} \langle b^1, b^1\rangle\right) c^0 - \sum_{a_0 \| c_0 b^1 = \mathcal{E}(a^0, c^0)} \frac{\langle b^1, b^1\rangle}{\langle a^0, a^0\rangle} a^0,
\end{aligned} \tag{15}$$

where $a_0 \parallel c_0$ means that a_0 and c_0 share a common edge, and $\mathcal{E}(a^0, c^0)$ is the basis 1-cochain corresponding to that edge.

Hodge star operator Let $q = d - p$ and

$$\star_p c^p = \sum_{b^q \in C^qK} \lambda_{b^q} b^q$$

for the unknowns $\lambda_{b^q} \in \mathbb{R}$. Then

$$(a^q \smile c^p)[K] = \langle a^q, \star_p c^p \rangle = \sum_{b^q} \lambda_{b^q} \langle a^q, b^q \rangle = \lambda_{a^q} \langle a^q, a^q \rangle.$$

Hence, $\lambda_{a^q} = (a^q \smile c^p)[K] / \langle a^q, a^q \rangle$ and therefore

$$\star_p c^p = \sum_{a^{d-p}} \frac{(a^{d-p} \smile c^p)[K]}{\langle a^{d-p}, a^{d-p} \rangle} a^{d-p}. \tag{16}$$

Evidently, the Hodge star is local, because nonzero numerators in the above summands are connected to the $(d-p)$-faces of the d-superfaces of c_p. An example with the contributors to the Hodge star of different cells is given in Fig. 3b.

$$\begin{aligned}
\star_0 N^{18} &= \frac{(F^5 \smile N^{18})[K]}{\langle F^5, F^5 \rangle} F^5 + \frac{(F^6 \smile N^{18})[K]}{\langle F^6, F^6 \rangle} F^6 + \frac{(F^{34} \smile N^{18})[K]}{\langle F^{34}, F^{34} \rangle} F^{34} + \frac{(F^{35} \smile N^{18})[K]}{\langle F^{35}, F^{35} \rangle} F^{35} \\
&= \frac{1}{4} \left(\frac{F^5}{\langle F^5, F^5 \rangle} + \frac{F^6}{\langle F^6, F^6 \rangle} + \frac{F^{34}}{\langle F^{34}, F^{34} \rangle} + \frac{F^{35}}{\langle F^{35}, F^{35} \rangle} \right). \\
\star_1 E^{33} &= \frac{(E^{33} \smile E^{38})[K]}{\langle E^{38}, E^{38} \rangle} E^{38} + \frac{(E^{33} \smile E^{43})[K]}{\langle E^{43}, E^{43} \rangle} E^{43} + \frac{(E^{33} \smile E^{78})[K]}{\langle E^{78}, E^{78} \rangle} E^{78} + \frac{(E^{33} \smile E^{84})[K]}{\langle E^{84}, E^{84} \rangle} E^{84} \\
&= \frac{1}{4} \left(\pm \frac{E^{38}}{\langle E^{38}, E^{38} \rangle} \pm \frac{E^{43}}{\langle E^{43}, E^{43} \rangle} \pm \frac{E^{78}}{\langle E^{78}, E^{78} \rangle} \pm \frac{E^{84}}{\langle E^{84}, E^{84} \rangle} \right). \\
\star_2 F^{45} &= \frac{(F^{45} \smile N^{13})[K]}{\langle N^{13}, N^{13} \rangle} N^{13} + \frac{(F^{45} \smile N^{15})[K]}{\langle N^{15}, N^{15} \rangle} N^{15} + \frac{(F^{45} \smile N^{40})[K]}{\langle N^{40}, N^{40} \rangle} N^{40} + \frac{(F^{45} \smile N^{56})[K]}{\langle N^{56}, N^{56} \rangle} N^{56} \\
&= \frac{1}{4} \left(\frac{N^{13}}{\langle N^{13}, N^{13} \rangle} + \frac{N^{15}}{\langle N^{15}, N^{15} \rangle} + \frac{N^{40}}{\langle N^{40}, N^{40} \rangle} + \frac{N^{56}}{\langle N^{56}, N^{56} \rangle} \right)
\end{aligned}$$

(the signs are generally different in the expression for $\star_1 E^{33}$ and depend on the orientation).

3.3. Orthogonal inner product via a metric tensor

Several discrete inner products have been proposed in the literature for topological studies, but these have not been developed in a canonical way by introduction of a discrete metric tensor and use of discrete Riemann integration. The canonical path is taken here by defining a class of discrete metric tensors. Two main variants are discussed: a trivial one and an extended one with curvature at nodes. The latter is used for the physical applications in Section 4.

For a cell $c_p \in K_p$ let $\mu(c_p)$ denote the geometric measure of c_p: 1 for 0-cells, length for 1-cells, area for 2-cells, and volume for 3-cells.

Definition 3.4. The discrete metric tensor $g_p : C^p K \times C^p K \to C^0 K$ is the unique bilinear map such that $g_p(b^p, c^p) = 0$ if $b^p \neq c^p$ and

$$g_p(c^p, c^p) := \frac{1}{\mu(c_p)^2} \frac{1}{2^p} \sum_{b^0 \preceq c^p} \kappa(b_0) b^0, \tag{17}$$

where $\kappa(b_0)$ is a dimensionless weight of b_0. Different choices will be discussed shortly.

Remark 3.5. While the metric tensor is defined for quasi-cubical meshes, the formula can be applied to simplicial meshes by replacing 2^p in the denominator with $p+1$ (the number of nodes of a simplex).

Definition 3.6. The volume cochain on K is the d-cochain

$$\mathrm{vol} := \sum_{c^d \in C^d K} \mu(c_d) c^d. \tag{18}$$

Definition 3.7. The inner product of p-forms, corresponding to the metric g, is the symmetric bilinear map $\langle \cdot, \cdot \rangle : C^p K \times C^p K \to \mathbb{R}$ defined by

$$\langle \sigma^p, \tau^p \rangle := (g(\sigma^p, \tau^p) \smile \mathrm{vol})[K]. \tag{19}$$

Obviously the map defined in Definition 3.7 is positive definite, i.e., it is indeed an inner product.

Remark 3.8. The physical dimensions of the constructed quantities are given in Table 1.

Remark 3.9. The definition of inner product is analogous to the one given in smooth Riemannian geometry. Indeed, define the Riemann integral of a 0-cochain f by

$$\int_K f \smile \mathrm{vol} := (f \smile \mathrm{vol})[K].$$

Table 1
Physical dimensions of discrete operators.

g_p	vol	$\langle\cdot,\cdot\rangle$	$\delta_p^\star$	Δ_p	$\star_p$
L^{-2p}	L^d	L^{d-2p}	$L^{(d-2p)-(d-2(p-1))} = L^{-2}$	L^{-2}	$L^{-(d-2(d-p))} = L^{d-2p}$

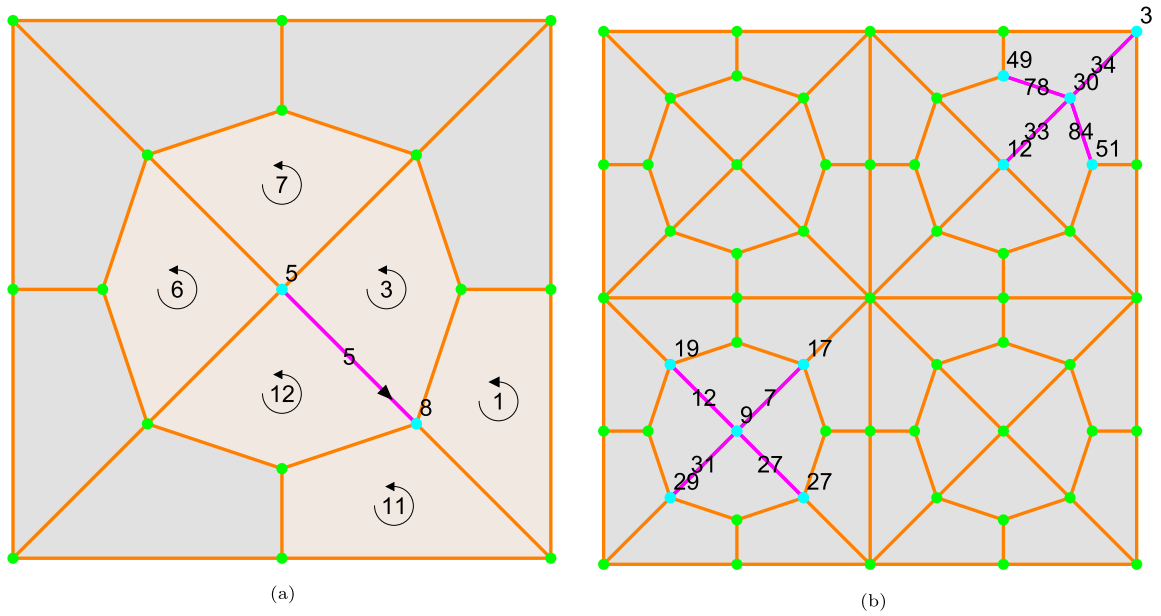

Fig. 4. Examples of: (a) inner product; (b) Laplacian.

Then

$$\langle \sigma^p, \tau^p \rangle = \int_K g(\sigma^p, \tau^p) \smile \mathrm{vol}\,.$$

Obviously $\langle a^p, b^p \rangle = 0$ if $a^p \neq b^p$. Otherwise,

$$\langle c^p, c^p \rangle = \frac{1}{2^p \mu(c_p)^2} \sum_{b_0 \preceq c_p} \kappa(b_0)(b^0 \smile \mathrm{vol})[K] = \frac{1}{2^{p+d}\mu(c_p)^2} \sum_{b_0 \preceq c_p} \kappa(b_0) \sum_{a_d \succeq b_0} \mu(a_d). \tag{20}$$

For a particular example of the contributors to the inner product, see Fig. 4a, where

$$\langle E^5, E^5 \rangle = \frac{1}{8\mu(E_5)^2}(\kappa(N_5)(\mu(F_3) + \mu(F_6) + \mu(F_7) + \mu(F_{12})) + \kappa(N_8)(\mu(F_1) + \mu(F_3) + \mu(F_{11}) + \mu(F_{12}))).$$

A trivial choice for the weights of 0-cells is $\kappa = 1$. This leads to some nice properties similar to the continuum case as shown by the following three examples.

1. $g(\overline{1_M}, c^0) = g\big(\sum_{a^0 \in C^0 K} a^0, c^0\big) = g(c^0, c^0) = c^0$. In particular, $g(\overline{1_M}, \overline{1_M}) = \overline{1_M}$.
2. Let $\mu(K) = \mu(M)$ be the measure of the whole region M and K represent. Then
$$\langle \overline{1_M}, \overline{1_M} \rangle = (\overline{1_M} \smile \mathrm{vol})[K] = \mathrm{vol}[K] = \mu(K) = \mu(M). \tag{21}$$
3. $\star_d \mathrm{vol} = \sum_{a^0} \frac{(a^0 \smile \mathrm{vol})[K]}{\langle a^0, a^0 \rangle} a^0 = \sum_{a^0} \frac{(a^0 \smile \mathrm{vol})[K]}{(a^0 \smile \mathrm{vol})[K]} a^0 = \sum_{a^0} a^0 = \overline{1_M}$.

While the choice $\kappa = 1$ for all 0-cells leads to known identities from smooth Riemannian geometry, and might be the appropriate choice for closed discrete manifolds, it is not suitable for discrete manifolds with boundary. The calculation of the adjoint coboundary operator close to the boundary requires special attention as illustrated with the following remark.

Remark 3.10. Consider M to be a partition of the interval $[0, 1]$ into $n \geq 2$ equal parts (in the picture below $n = 2$). Then K is the partition of $[0, 1]$ into $2n$ equal parts. Label the nodes from 0 to $2n$, the edges from 1 to $2n$, and orient all edges in the positive direction, i.e., $\varepsilon(E_i, N_{i-1}) = -1,\ \varepsilon(E_i, N_i) = 1,\ i = 1, \ldots, 2n$. Let $h = 1/(2n)$.

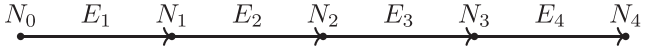

Since boundary nodes have only half the volumes around them,

$$\begin{aligned}&\langle N^i, N^i\rangle = h/2,\ \ i \in \{0, 2n\}\\ &\langle N^i, N^i\rangle = h,\ \ i \in \{1, \dots, 2n-1\}\end{aligned}\ ,$$

$$\begin{aligned}&\langle E^i, E^i\rangle = \tfrac{1}{2h^2}(h/2+h) = \tfrac{3}{4h},\ \ i \in \{1, 2n\}\\ &\langle E^i, E^i\rangle = \tfrac{1}{2h^2}(h+h) = \tfrac{1}{h},\ \ i \in \{2, \dots, 2n-1\}\end{aligned}\ .$$

Hence, on the one hand

$$\begin{aligned}\Delta_0 N^2 &= \frac{1}{\langle N^2, N^2\rangle}(\langle E^2, E^2\rangle + \langle E^3, E^3\rangle)N^2 - \frac{\langle E^2, E^2\rangle}{\langle N^1, N^1\rangle}N^1 - \frac{\langle E^3, E^3\rangle}{\langle N^3, N^3\rangle}N^3\\ &= \frac{1/h + 1/h}{h/2}N^2 - \frac{1/h}{h}N^1 - \frac{1/h}{h}N^3\\ &= \frac{1}{h^2}\left(2N^2 - N^1 - N^3\right),\end{aligned}$$

which has the same form as the finite difference Laplacian. However, on the other hand

$$\begin{aligned}\Delta_0 N^1 &= \frac{1}{\langle N^1, N^1\rangle}(\langle E^1, E^1\rangle + \langle E^2, E^2\rangle)N^1 - \frac{\langle E^1, E^1\rangle}{\langle N^0, N^0\rangle}N^0 - \frac{\langle E^2, E^2\rangle}{\langle N^2, N^2\rangle}N^2\\ &= \frac{3/(4\ h) + 1/h}{h/2}N^1 - \frac{3/(4\ h)}{h/2}N^0 - \frac{1/h}{h}N^2\\ &= \frac{1}{h^2}\left(\frac{7}{8}N^1 - \frac{3}{8}N^0 - N^2\right),\end{aligned}$$

which is not what is expected from an interior node. The problem arises when the Laplacian acting on a node adjacent to the boundary uses the inner product of a boundary 0-cochain with itself, which does not have all the volumes around. This is typical for any regular grid: the equations corresponding to interior nodes which do not have boundary neighbours are given by (minus) the finite difference Laplacian, but the equations corresponding to boundary nodes and almost boundary nodes (nodes with boundary neighbours) are different.

For a 2D example, see Fig. 4b. The vertex N_9 has full volumes around its neighbouring cells, and so full Laplacian

$$\begin{aligned}\Delta_0 N^9 = &\frac{1}{\langle N^9, N^9\rangle}(\langle E^7, E^7\rangle + \langle E^{12}, E^{12}\rangle + \langle E^{27}, E^{27}\rangle + \langle E^{31}, E^{31}\rangle)N^9\\ &- \frac{\langle N^{17}, N^{17}\rangle}{\langle E^7, E^7\rangle}N^{17} - \frac{\langle N^{19}, N^{19}\rangle}{\langle E^{12}, E^{12}\rangle}N^{19} - \frac{\langle N^{27}, N^{27}\rangle}{\langle E^{27}, E^{27}\rangle}N^{27} - \frac{\langle N^{29}, N^{29}\rangle}{\langle E^{31}, E^{31}\rangle}N^{29}.\end{aligned}$$

The Laplacian at N^{30} is:

$$\begin{aligned}\Delta_0 N^{30} = &\frac{1}{\langle N^9, N^9\rangle}(\langle E^{33}, E^{33}\rangle + \langle E^{34}, E^{34}\rangle + \langle E^{78}, E^{78}\rangle + \langle E^{84}, E^{84}\rangle)N^{30}\\ &- \frac{\langle N^{12}, N^{12}\rangle}{\langle E^{33}, E^{33}\rangle}N^{12} - \frac{\langle N^3, N^3\rangle}{\langle E^{34}, E^{34}\rangle}N^3 - \frac{\langle N^{49}, N^{49}\rangle}{\langle E^{78}, E^{78}\rangle}N^{49} - \frac{\langle N^{51}, N^{51}\rangle}{\langle E^{84}, E^{84}\rangle}N^{51}.\end{aligned}$$

Because N_3 is on the boundary, $\langle N^3, N^3\rangle$ and $\langle E^{34}, E^{34}\rangle$ will have less contributions from surrounding volumes and $\Delta_0 N^{30}$ is not "full" Laplacian.

This problem is addressed here by selecting the weights of 0-cells to be equal to 0-cell curvatures defined as follows. Let A be an affine space. For $z_0 \in A$ and $r \in \mathbb{R}^+$ let $\S_{d-1}(c_0, r)$ be the sphere with centre c_0 and radius r, $\S_{d-1}(1)$ be the unit sphere with any centre (its measure, used below, does not depend on the centre).

Definition 3.11. Let c_d be a d-polytope with affine hull A, a_0 be a node of c_d, Θ be the cone in A centered at a_0 and bounded by the edges starting from a_0. Let $\S_{d-1}(a_0, r)$ be the $(d-1)$-sphere in A centered at a_0 with radius r, i.e., the boundary of the corresponding d-ball. The angle measure $\angle(c_d, a_0)$ of Θ is defined as the ratio between the surface measure of $\Theta \cap \S_{d-1}(a_0, r)$ and $\S_{d-1}(a_0, r)$. The definition does not depend on the radius r because both measures are proportional to r^{d-1}.

Remark 3.12. If $d = 0$, then Θ is always 1; if $d = 1$, then Θ is always $1/2$; if $d = 2$, then Θ is the radian measure of a planar angle (between 0 and 2π and less than π for convex polygons); if $d = 3$, then Θ is the steradian measure of a solid angle (between 0 and 4π and less than 2π for convex polyhedrons).

Definition 3.13. Let K be a d-mesh embeddable in $\mathbb{R}^d$ and a_0 be a node in K. The (node) curvature of a_0, and therefore its weight in the metric tensor, is defined by

$$\kappa(a_0) = \frac{\mu(\S_{d-1}(1))}{\sum_{c_d \geq a_0} \angle(c_d, a_0)} \in [1, \infty). \tag{22}$$

Remark 3.14. The curvature of an interior node of K is always 1; the curvature of a boundary node is different from 1. Consider, for example, the case of a cubical domain. If a_0 lies on a domain face, but not on a domain edge, its curvature is 2. If a_0 lies on a domain edge, but not on a domain corner, its curvature is 4. If a_0 is a domain corner, its curvature is 8.

For a regular grid this choice of κ leads to the same Laplacian as in the finite difference method for all interior nodes. The equations at the boundary also have nice form for such a grid, but are not presented here, as the theory is developed and valid for general polyhedral meshes.

4. Applications

Applied to 0-forms, the Laplacian has the form $\Delta = \delta^\star \circ \delta$, explicitly given by Eq. (15). The discrete version of the heat/diffusion equation is obtained by introducing the physical property, diffusivity, to modify the Laplacian to

$$\Delta_0^\alpha := \delta_1^\star \circ \alpha \circ \delta_0, \tag{23}$$

where $\alpha : C^1\ K \to C^1 K$ is a symmetric positive definite map. Specifically for the examples in this work, it is assumed that $\alpha(b^1) = \alpha_{b^1} b^1$, where $\alpha_{b^1} > 0$ is the local diffusivity of cell b_1. In such case the exact formula for $\Delta_0^\alpha c^0$ is calculated analogously to Eq. (15) and reads

$$\Delta_0^\alpha c^0 = \frac{1}{\langle c^0, c^0\rangle}\left(\sum_{b_1 \succ c_0} \alpha_{b^1} \langle b^1, b^1\rangle\right) c^0 - \sum_{\substack{a_0 \| c_0 \\ b^1 = \mathcal{E}(a^0, c^0)}} \alpha_{b^1} \frac{\langle b^1, b^1\rangle}{\langle a^0, a^0\rangle} a^0. \tag{24}$$

The construction of K from M provides three types of 1-cells in K associated with: (1) pairs $(b_0 \prec b_1) \in M$ (i.e., along 1-cells/edges of M); (2) pairs $(b_1 \prec b_2) \in M$ (i.e., along 2-cells/faces of M); and (3) pairs $(b_2 \prec b_3) \in M$ (i.e., through 3-cells/volumes of M). Considering that M is a representation of a material with internal structure, the three types of 1-cells in K allow for associating different diffusivity to components of M with different geometric dimensions. This provides a considerable advantage for the proposed theory - simultaneous analysis of processes taking place with different rates on microstructural components of different dimensions - which cannot be accomplished with numerical methods based on the continuum formulation.

The discrete version of the heat/diffusion equation without body sources reads

$$\frac{\partial \sigma^0}{\partial t} = \Delta_0^\alpha \sigma^0, \tag{25}$$

where σ^0 is the 0-cochain of the unknown scalar variable. Importantly, in the discrete formulation the fluxes correspond to area integrated continuum fluxes, i.e., to the total fluxes rather than to flux densities used in Section 1.1. Specifically, the discrete flux along a 1-cell, b_1 is given by

$$f(b_1) = -\alpha_{b^1} \langle b^1, b^1\rangle\ (\delta_0 \sigma^0)(b_1), \tag{26}$$

with physical dimension $[f] = [\sigma^0] L^3/T$.

All mathematical operations described in the paper, leading to the system Eq. (25) are implemented in MATLAB and the code is available at: https://github.com/boompiet/Forman_MATLAB. This repository contains also the meshes used for the simulations described in the following sub-sections.

4.1. Numerical simulations

Simple numerical simulations are presented to highlight some of the features of the proposed theory. These include simulations on regular-orthogonal and quasi-random meshes to show the influence of geometric variation, as well as application to electrical diffusivity of a composite including graphene nano-plates (2D) and carbon nano-tubes (1D) in a polymer matrix (3D) to demonstrate simultaneous simulation on elements of different geometric dimensions. The quasi-random meshes are generated using the freely available software for Voronoi-type tessellations Neper: https://neper.info.

Dirichlet boundary conditions are applied by multiplying the columns of the system matrix associated with points on the given boundary by the prescribed values and subtracting the sum from the left-hand side of the equation. The rows and columns of the system associated with these points are then removed before final solution. Neumann boundary conditions are in principle applied by prescribing fluxes, but the example considered here involve zero fluxes, hence no modification of the system of equations was required. The solution of the transient problem, given by Eq. (25), can be obtained by a standard time integration scheme. However, it has been confirmed separately that the transient solutions reach the steady-state results, albeit after different time intervals, depending on the mesh and prescribed local diffusivity coefficients. For computational efficiency, the results presented hereafter are obtained by steady-state solutions.

Following solution of the system, the flux through a domain boundary surface with Dirichlet boundary condition is computed by

$$F = \sum_{b_1} |f(b_1)|, \tag{27}$$

Table 2
Flux (effective diffusivity) of regular and irregular meshes, broken down by the contribution from each type of 1-cell in K.

	Edge type, n, in K:	Value of flux (effective diffusivity)	
	$c_n \to c_{n+1} \in M$	$z = 0$	$z = 1$
Regular	All	1.0506	1.0506
	0	0.2756	0.2756
	1	0.5250	0.5250
	2	0.2500	0.2500
Irregular	All	1.1604	1.1604
	0	0.1959	0.1959
	1	0.5238	0.5238
	2	0.3752	0.3752

where the sum is taken over all 1-cells with one interior and one surface 0-cell. The calculation of the effective diffusivity of a material domain is analogous the experimental determination of such a parameter. Dirichlet boundary conditions with different values, u_0 and $u_1 > u_0$, are applied at two parallel boundary surfaces, which are at normal distance h and have area A. With the calculated flux at either boundary, the effective diffusivity is given by

$$\alpha_{\text{eff}} = \frac{Fh}{(u_1 - u_0)A}, \tag{28}$$

where $[\alpha_{\text{eff}}] = L^2/T$.

4.2. Diffusion on regular and irregular meshes

To compare the influence of geometric regularity, we consider the diffusion of a scalar quantity through a unit cube. The diffusion coefficient associated with all 1-cells in K is unity. Dirichlet boundary conditions are applied to the top surface with unit value and to the bottom surface with a zero value. On the remaining four exterior surfaces, zero flux Neumann boundary conditions are enforced. With this setup, the computed fluxes at the top and bottom surface equal in numerical values the effective diffusivity of the domain.

One example uses a regular mesh M composed of $20 \times 20 \times 20 = 8,000$ cubic cells, leading to a cubical mesh K with 68,921 vertices and 201,720 edges. A second example uses irregular mesh M composed of 2500 Voronoi cells, leading to a quasi-cubical mesh with 68,545 vertices and 194,466 edges. The M meshes are shown in Fig. 5.

The variation of the scalar variable as a function of z-coordinate is shown in Fig. 6. On the regular grid (left) the result is identical to finite differences, as well as discrete exterior calculus, and exactly reproduces the linear profile of the continuum solution. The solution values on the irregular grid (center) are scattered (right) about the continuum solution, highlighting the influence of the meshes underlying geometry. It needs to be emphasised that the analytical solution is based on the continuum description of diffusion, while the simulations are based on a formulation of balance of scalar quantity intrinsic to a discrete topology. As a result, the cells of different topological dimensions do contribute to the diffusion. Evidence for how these control macroscopic behaviour are the computed fluxes (effective diffusivity) for the regular and irregular meshes given in Table 2. The fluxes are broken down by the contribution from each type of 1-cell in K, representing different cells in M. It is clear, that while the spatial distribution of the quantity follows exactly (Fig. 6 — left) or with small deviations (Fig. 6 — right) the analytical result from a continuum formulation, the internal structure has a strong impact on the effective diffusivity. In the analytical solution there is no difference between local and effective diffusivity coefficients. In a material with an internal structure, different components contribute differently to the effective diffusivity, which in both cases is found larger than unity.

The fact that in this example the diffusivity coefficients of the cells with different dimensions are equal does not mean homogeneity in continuum sense, as there is a well defined underlying discrete structure directing the diffusion. The agreement between the steady-state spatial distribution of the analysed quantity with a regular mesh with the analytical solution (and the classical finite difference scheme) only shows that a completely regular internal structure with constant local diffusivity is indistinguishable from a continuum. However, a divergence from regularity in the internal structure leads to deviations of the steady-state spatial distribution of the quantity from the continuum result, even for constant local diffusivity values - a demonstration of how structure controls behaviour.

To clarify this point further, an investigation of the effect of cell size, analogous to a mesh convergence study, was also carried out, and the results are shown in Table 3. In both the regular and irregular meshes, the flux (effective diffusivity) is decreasing with decreasing ratio between cell and system sizes. This is an indication that the continuum formulation provides a lower limit for the diffusivity of a solid, namely a diffusivity of a structure-less solid. Notably, this should not be considered as a convergence to a continuum solution, but rather an indication that the continuum is an approximation for materials with structures when the internal arrangements are “forgotten”. It is an increasingly good approximation with increasing number of cells in an assembly. Regarding the different rates of flux reduction with cell size, note that while the

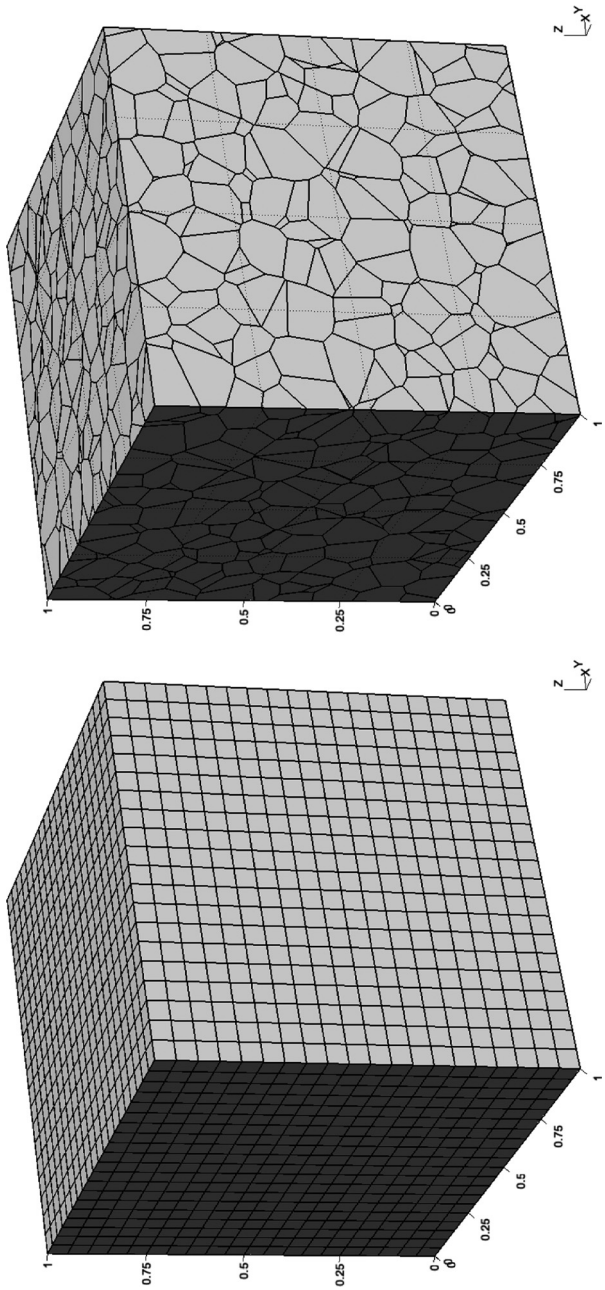

Fig. 5. Regular and irregular meshes (extended complex not shown).

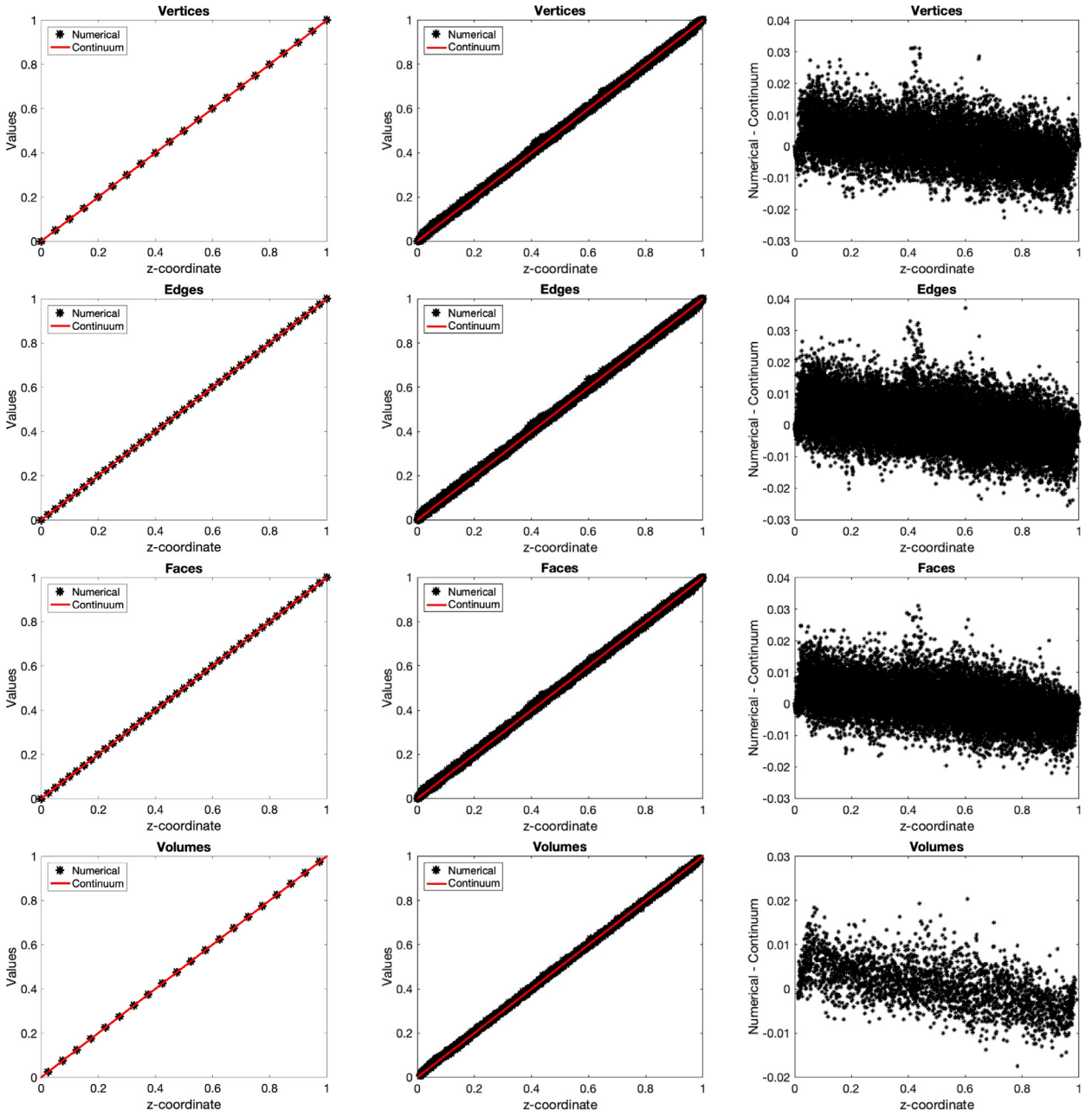

Fig. 6. Value of scalar variable at vertices, edges, faces and volumes in M (vertices of K) plotted as a function of z-coordinate for both regular (left) and irregular (center) meshes. Also shown (right) is the scatter of the numerical solution on the irregular mesh about the continuum solution.

regular meshes do form a natural family of nested meshes, the irregular meshes are generated independently for a given number of cells in M.

4.3. Effective diffusivity of composites with graphene nano-plates and carbon nano-tubes

After clarifying the effect of different components of M on the effective property of M, the proposed theory is applied to a practical engineering problem: electrical diffusivity of a composite with a polymer or a ceramic matrix (3D) and dispersed graphene nano-plates (GNP, 2D) or carbon nano-tubes (CNT, 1D). The matrix has a low electrical diffusivity, whereas the GNP and the CNT have substantially higher electrical diffusivity. It is expected that at a given (mass/volume) fraction of GNP or CNT, the composite will exhibit a sharp increase in effective diffusivity, as the dispersed inclusions form a percolating

Table 3
The effect of cell size on the value of flux (effective diffusivity) computed on regular and irregular meshes.

	Number of cell in M	Value of flux (effective diffusivity)	
		$z = 0$	$z = 1$
Regular	2^3	1.5625	1.5625
	4^3	1.2656	1.2656
	8^3	1.1289	1.1289
	16^3	1.0635	1.0635
	32^3	1.0315	1.0315
Irregular	8	1.3754	1.3754
	64	1.2490	1.2490
	512	1.1815	1.1815
	4096	1.1524	1.1524
	32768	1.1406	1.1406

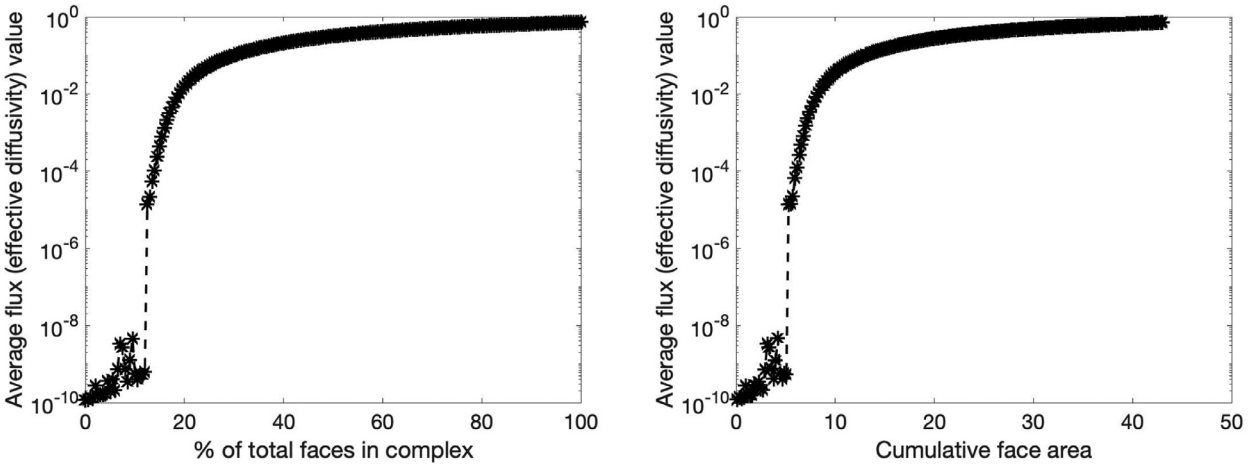

Fig. 7. Effective diffusivity of GNP composite as a function of: fraction of faces covered by GNP (left); and cumulative area of GNPs (right).

path across the domain. While analysis of percolation is not new in the studies of critical phenomena, the theory developed in this work allows for quantitative analysis of the macroscopic property in question - effective diffusivity.

For these simulations, the 3-cells of M contain the polymer matrix, and the 1-cells of K inside these 3-cells are assigned a negligible electrical diffusivity of 10^{-10}. For a composite with GNP, the nano-plates reside on select 2-cells of M, and the 1-cells of K inside these 2-cells and along their boundary 1-cells are assigned an electrical diffusivity of 1. For a composite with CNT, the nano-tubes reside on select 1-cells of M, and the 1-cells of K along these 1-cells are assigned an electrical diffusivity of 1.

Simulations are performed with the same irregular mesh from the previous case. The faces and edges representing the GNP and CNT, respectively, are selected from a random uniform distribution of integers without replacement. Selected faces or edges are added successively from 0% to 100% of the total number. 200 Monte Carlo paths are run to obtain a statistical average flux (effective diffusivity) for the composite as a function of percent number or volume/mass fraction.

It should be noted here that introducing diffusion coefficients varying by 10 orders of magnitude, coupled with cell volumes, face areas and edge lengths varying by 2, 9 and 5 orders of magnitude, respectively, can lead to a system that is poorly conditioned. The degree to which the system is poorly conditions depends on the specific combination of faces and edges that are assigned the higher diffusion coefficient. The result of this poor conditioning is visible as spikes in the data plotted in this section. Ongoing work includes developing strategies to mitigate this numerical stiffness.

The evolution of average effective diffusivity with dispersed GNP is shown in Fig. 7 as functions of the fraction of 2-cells covered by GNP and of total GNP area. The expected step change in effective electrical diffusivity of the composite is recovered. The fraction of 2-cells covered by GNP at the step change, referred to as the percolation threshold, is consistent with results presented in [33] for nano-composites with ceramic matrix and graphene-oxide inclusions. Experimentally, the percolation threshold has been determined in terms of the inclusions' volume fraction, ϕ, and has varied between 0.38% and 7.3% [34]. The particular value determined in [34] is $\phi = 1.18\%$. For an average plate/inclusion thickness t (dimension L), and a given area covered by GNP at percolation A_c (non-dimensional), a simple calculation shows that a percolation threshold ϕ re-scales the unit cube to edge length $L_c = A_c \cdot t/\phi$ (dimension L). This gives an average 3-cell size $d = L_c/2500^{1/3}$, which is also approximately equal to the average in-plane diameter of GNP. Considering $A_c \approx 8$ units from Fig. 7, $d \approx 0.589\, t/\phi$.

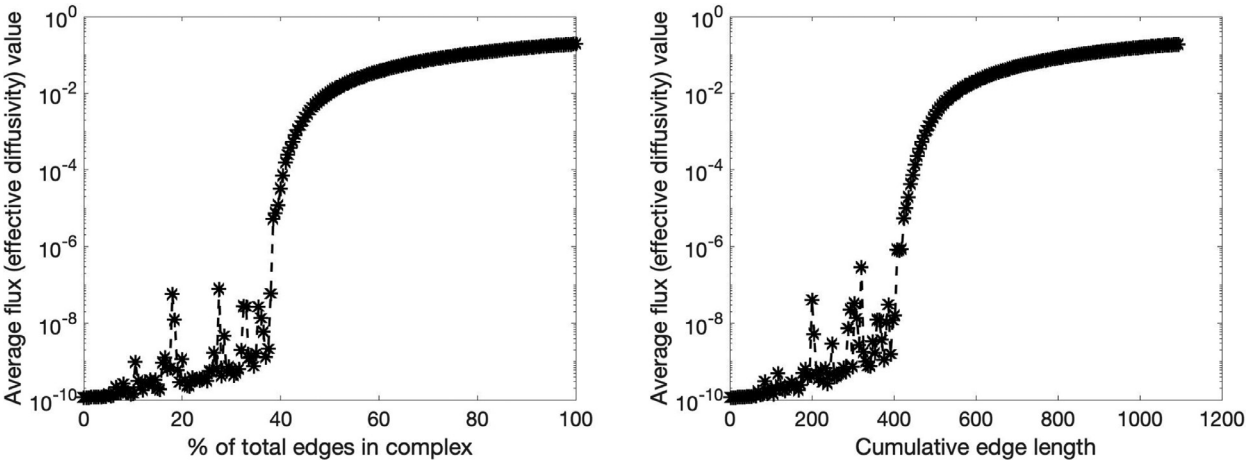

Fig. 8. Effective diffusivity of CNT composite as a function of: fraction of edges covered by CNT (left); and cumulative length of CNTs (right).

Assuming an average plate thickness $t = 3\,nm$ [33] this gives the following GNP diameters: $d = 465\,nm$ for $\phi = 0.38\%$; $d = 150\,nm$ for $\phi = 1.18\%$; and $d = 24\,nm$ for $\phi = 7.3\%$. The result suggests an explanation for the different volume fraction thresholds reported in the literature: the sizes of GNP used in different experiments were different. As observed previously [33], the effective conductivity can be increased by larger plates with lower volume fraction.

The evolution of the average effective diffusivity of the composite with dispersed CNT is shown in Fig. 8. The expected step change is still clearly visible, but occurs at a much higher fraction of 1-cells covered by CNT. Experimental data for polymer composite with carbon nano-tubes [35] shows that the percolation threshold is around 0.5 wt%. Considering the polymer density $\rho_p = 1.07 g/m^3$ and the CNT density $\rho_c = 2.16 g/m^3$ reported in [35], this translates into a CNT volume fraction at percolation $\phi = 1\%$. For an average nano-tube radius r (dimension L), and a given length of 1-cells occupied by CNT at percolation L_c (non-dimensional), a calculation similar to the last one shows that a percolation threshold ϕ re-scales the unit cube to face area $A_c = L_c \cdot \pi \cdot r^2/\phi$ (dimension L^2). This gives an average 3-cell size $d = A^{1/2}/2500^{1/3}$, which is also approximately equal to the average CNT length. Considering $L_c \approx 450$ from Fig. 8, $d \approx 2.77\, r/\phi^{1/2}$. For the measured CNT volume fraction at percolation $\phi = 1\%$, the relation between length and radius of CNT is $d \approx 27.7\, r$, suggesting that the experiment was performed with relatively short CNT. Generally, the diameter of CNT can vary from less than $1\,nm$ to over $100\,nm$, and the length can vary from several nano-metres to several centimetres. Taking example from the case with GNP, it can be suggested that the effective diffusivity can be increased by longer nano-tubes with lower volume fraction.

5. Conclusions

The paper presented a geometric development of Forman's combinatorial formulations of discrete differential forms and exterior derivatives of such forms on discrete topological spaces. The development is based on the isomorphism between the space of differential p-forms in a given d-complex and the space of p-cochains in an extended d-complex. The coboundary operators on cochains in the extended complex represent the exterior derivatives of forms in the given complex. Notably, the given complex is required to be an assembly of simple d-polytopes, i.e., each vertex of every d-polytope is adjacent to exactly d edges of that polytope. This requirement is fulfilled not only by the most widely used simplicial complexes, but also by polyhedral complexes arising from different Voronoi tessellations of space. Under such a requirement, the extended d-complex is quasi-cubical, which allows for construction of exterior (wedge) product of forms in the given complex as cup product of cochains in the extended complex. The key contributions of the work are the introduction of a metric tensor as a proper bi-linear map from p-cochains to 0-cochains and the use of discrete Riemann integration to define inner product in the space of p-cochains. The resulting adjoint coboundary operator, Laplacian, and Hodge-star operator, are constructed canonically for a given discrete space, and do not rely on a construction of a dual mesh as in the existing discrete exterior calculus. The use of combinatorial differential forms has two consequences. First, the formulation of balance laws is intrinsic, i.e., it does not depend on the existence of smooth external fields. Second, the cells with different topological dimensions in the given complex can be used to represent components of materials' internal structures with different (apparent) geometric dimensions, which in many practical cases have different physical properties. For example, prescribing different diffusivity coefficients to 1-cells, 2-cells, and 3-cells of the given complex, changes the diffusion rate along lines, surfaces, and through volumes.

The complete theory is applied to analysis of charge diffusion in two types of composites: polymer composites with dispersed graphene nano-plates; and ceramic composites with dispersed carbon nano-tubes. In the former case, the conductive inclusions form a subset of the set of 2-cells. In the latter case, the conductive inclusions from a subset of the set of 1-cells. In both cases, the fraction of dispersed inclusions is varied between 0 and 100% to capture the percolation thresh-

old, i.e., the fraction at which the measured charge flux changes sharply. By comparing the calculated percolation thresholds with experimentally measured values, it is suggested that the large differences in the experimental values are likely due to different sizes of the inclusions used for manufacturing the composites. For example, experimentally measured thresholds for graphene nano-plates between 0.38% and 7.3% require nano-plates with diameters between $465\,nm$ and $24\,nm$ - lower volume fraction require larger nano-plates for percolation. Similarly, it is concluded that lower volume fraction of carbon nano-tubes require longer nano-tubes for percolation.

The work offers a background-independent formulation of balance of scalar quantities and is the first important step towards a background-independent formulation of balance of momenta in discrete topological spaces, which includes problems in solid and fluid mechanics. This is a subject of ongoing investigation.

Declaration of Competing Interest

The authors declare no conflict of interests.

Acknoledgements

This document is a result of a research sponsored by Engineering and Physical Sciences Research Council via grant EP/N026136/1.

Supplementary material

Supplementary material associated with this article can be found, in the online version, at doi:10.1016/j.apm.2022.05.043.

References

[1] P. Boisse, Composite Reinforcements for Optimum Performance, Elsevier, London, 2021. Available from: https://www.sciencedirect.com/book/9780128190050/composite-reinforcements-for-optimum-performance.
[2] K.K. Sankaran, R.S. Mishra, Metallurgy and Design of Alloys with Hierarchical Microstructures, Elsevier, London, 2017. Available from: https://www.sciencedirect.com/book/9780128120682/metallurgy-and-design-of-alloys-with-hierarchical-microstructures.
[3] T. DebRoy, H. Wei, J. Zuback, T. Mukherjee, J. Elmer, J. Milewski, et al., Additive manufacturing of metallic components – process, structure and properties, Prog. Mater. Sci. 92 (2018) 112–224. Available from: https://www.sciencedirect.com/science/article/abs/pii/S0079642517301172.
[4] T. Ngo, A. Kashani, G. Imbalzano, K. Nguyen, D h. additive manufacturing (3D printing): a review of materials, methods, applications and challenges, Compos. Part B 143 (2018) 172–196. Available from: https://www.sciencedirect.com/science/article/abs/pii/S1359836817342944.
[5] B.J. West, Nature's Patterns and the Fractional Calculus, de Gruyte, Berlin, 2017. Available from: https://www.degruyter.com/document/doi/10.1515/9783110535136/html.
[6] H.G. Sun, Y. Zhang, D. Baleanu, W. Chen, Y.Q. Chen, A new collection of real world applications of fractional calculus in science and engineering, Commun. Nonlinear Sci. Numer. Simul. 64 (2018) 213–231. Available from: https://www.sciencedirect.com/science/article/abs/pii/S1007570418301308.
[7] H. Sherief, A. El-Sayed, A. Abd El-Latief, Fractional order theory of thermoelasticity, Int. J. Solids Struct. 47 (2010) 269–275. Available from: https://www.sciencedirect.com/science/article/pii/S002076830900376X.
[8] M. Di Paola, A. Pirrotta, A. Valenza, Visco-elastic behavior through fractional calculus: an easier method for best fitting experimental results, Mech. Mater. 43 (2011) 799–806. Available from: https://www.sciencedirect.com/science/article/abs/pii/S0167663611001657.
[9] M. Bologna, A. Svenkeson, B. West, P. Grigolini, Diffusion in heterogeneous media: an iterative scheme for finding approximate solutions to fractional differential equations with time-dependent coefficients, J. Comput. Phys. 293 (2015) 297–311. Available from: https://www.sciencedirect.com/science/article/pii/S0021999114005816.
[10] M. Singh, S. Das, E.M. Craciun, et al., Numerical solution of two-dimensional nonlinear fractional order reaction-advection-diffusion equation by using collocation method, Analele Stiintifice ale Universitatii Ovidius Constanta 29 (2) (2021) 211–220. Available from: https://sciendo.com/article/10.2478/auom-2021-0027.
[11] M. Alharthi, T. Marchant, M. Nelson, Mixed quadratic-cubic autocatalytic reaction–diffusion equations: semi-analytical solutions, Appl. Math. Model. 38 (21–22) (2014) 5160–5173. Available from: https://www.sciencedirect.com/science/article/pii/S0307904X14001978.
[12] A. Hirani, Discrete exterior calculus, California Institute of Technology, 2003 [Ph.D. thesis]. Available from: https://thesis.library.caltech.edu/1885/.
[13] D. Arnold, Finite Element Exterior Calculus. Vol. 93 of CBMS-NSF Regional Conference Series in Applied Mathematics, Society for Industrial and Applied Mathematics (SIAM), Philadelphia, PA, 2018. Available from: https://epubs.siam.org/doi/book/10.1137/1.9781611975543.
[14] A. Hirani, K. Nakshatrala, J. Chaudhry, Numerical method for Darcy flow derived using discrete exterior calculus, Int. J. Comput. Methods Eng. Sci. Mech. 16 (3) (2015) 151–169. Available from: https://www.tandfonline.com/doi/full/10.1080/15502287.2014.977500.
[15] M. Mohamed, A. Hirani, R. Samtaney, Discrete exterior calculus discretization of incompressible Navier–Stokes equations over surface simplicial meshes, J. Comput. Phys. 312 (2016) 175–191. Available from: https://www.sciencedirect.com/science/article/pii/S0021999116000929.
[16] E. Schulz, G. Tsogtgerel, Convergence of discrete exterior calculus approximations for poisson problems, Discrete Comput. Geom. 63 (2020) 364–376. Available from: https://link.springer.com/article/10.1007/s00454-019-00159-x.
[17] P. Boom, O. Kosmas, L. Margetts, A. Jivkov, A geometric formulation of linear elasticity based on discrete exterior calculus, Int. J. Solids Struct. 236–237 (2022) 111345. Available from: https://www.sciencedirect.com/science/article/abs/pii/S0020768321004212.
[18] J. Bonelle, Compatible discrete operator schemes on polyhedral meshes for elliptic and Stokes equations, Université Paris-Est, 2014 [Ph.D. thesis]. Available from: https://cermics.enpc.fr/cermics-theses/2014/2014/bonelle.pdf.
[19] L.B. Da Veiga, F. Brezzi, L.D. Marini, A. Russo, $H(\mathrm{div})$ and $H(\mathrm{curl})$-conforming virtual element methods, Numer. Math. 133 (2) (2016) 303–332. Available from: https://link.springer.com/article/10.1007/s00211-015-0746-1.
[20] D.A. Di Pietro, J. Droniou, An arbitrary-order discrete de Rham complex on polyhedral meshes: exactness, Poincaré inequalities, and consistency, Found. Comput. Math. (2021) 1–80. Available from: https://link.springer.com/content/pdf/10.1007/s10208-021-09542-8.pdf.
[21] E. Tonti, The Mathematical Structure of Classical and Relativistic Physics: A General Classification Diagram, Springer, 2013. Available from: https://link.springer.com/book/10.1007.
[22] R. Forman, Morse theory for cell complexes, Adv. Math. 134 (1998) 90–145. Available from: https://www.sciencedirect.com/science/article/pii/S0001870897916509.
[23] R. Forman, Combinatorial Novikov-Morse theory, Int. J. Math. 13 (4) (2002) 333–368. Available from: https://www.worldscientific.com/doi/abs/10.1142/S0129167X02001265.

[24] S. Harker, K. Mischaikow, M. Mrozek, V. Nanda, Discrete morse theoretic algorithms for computing homology of complexes and maps, Found. Comput. Math. 14 (1) (2014) 151–184. Available from: https://link.springer.com/article/10.1007.
[25] M. Mrozek, T. Wanner, Creating semiflows on simplicial complexes from combinatorial vector fields, J. Differ. Equ. 304 (2021) 375–434. Available from: https://www.sciencedirect.com/science/article/abs/pii/S0022039621006069.
[26] R. Forman, Bochner's method for cell complexes and combinatorial RICCI curvature, Discrete Comput. Geom. 29 (3) (2003) 323–374. Available from: https://link.springer.com/article/10.1007/s00454-002-0743-x.
[27] C.E.M.C. Lange, Combinatorial curvatures, group actions, and colourings: aspects of topological combinatorics, Technical University of Berlin, 2005 [Ph.D. thesis]. Available from: https://depositonce.tu-berlin.de/handle/11303/1149.
[28] K. Watanabe, Combinatorial Ricci curvature on cell-complex and gauss-bonnet theorem, Tohoku Math. J. 71 (2019) 533–547. Available from: https://projecteuclid.org/journals/tohoku-mathematical-journal/volume-71/issue-4/Combinatorial-Ricci-curvature-on-cell-complex-and-Gauss-Bonnnet-theorem/10.2748/tmj/1576724792.short.
[29] M. Weber, J. Jost, E. Saucan, Forman-Ricci flow for change detection in large dynamic data sets, Axioms 5 (4) (2016) 26. Available from: https://www.mdpi.com/2075-1680/5/4/26.
[30] R.F. Arnold, The discrete hodge star operator and poincaré duality, Virginia Tech, 2012 [Ph.D. thesis]. Available from: https://vtechworks.lib.vt.edu/handle/10919/27485.
[31] S.O. Wilson, Cochain algebra on manifolds and convergence under refinement, Topol. Appl. 154 (9) (2007) 1898–1920. Available from: https://www.sciencedirect.com/science/article/pii/S0166864107000314.
[32] H. Whitney, Geometric Integration Theory, Princeton University Press, 1957. Available from: https://press.princeton.edu/books/hardcover/9780691652900/geometric-integration-theory.
[33] A. Borodin, A. Jivkov, A. Sheinerman, G. MYu, Optimisation of rGO-enriched nanoceramics by combinatorial analysis, Mater. Des. 212 (2021) 110191. Available from: https://www.sciencedirect.com/science/article/pii/S0264127521007462.
[34] A. Nistal, E. Garcia, D. Perez-Coll, C. Prieto, M. Belmonte, M. Osendi, et al., Low percolation threshold in highly conducting graphene nanoplatelets/glass composite coatings, Carbon 139 (2018) 556–563. Available from: https://www.sciencedirect.com/science/article/abs/pii/S0008622318306729.
[35] C. Micaela, R. Massimo, S. Muhammad Imran, T. Alberto, Conductivity in carbon nanotube polymer composites: a comparison between model and experiment, Compos.Part A 87 (2016) 237–242. Available from: https://www.sciencedirect.com/science/article/abs/pii/S1359835X16301208.